The Cooling of Compact Stars

Dany Page, Ulrich Geppert and Fridolin Weber

November 2006

Publication Number: CSRCR2006-24

Computational Science & Engineering Faculty and Students Research Articles

Database Powered by the Computational Science Research Center Computing Group

COMPUTATIONAL SCIENCE & ENGINEERING

SAN DIEGO STATE UNIVERSITY

Computational Science Research Center
College of Sciences
5500 Campanile Drive
San Diego, CA 92182-1245
(619) 594-3430

The Cooling of Compact Stars

Dany Page[1] [a], Ulrich Geppert [b], Fridolin Weber[2] [c]

[a] *Departamento de Astrofísica Teórica, Instituto de Astronomía, Universidad Nacional Autónoma de México, 04510 Mexico D.F.*

[b] *Max-Planck-Institut für extraterrestrische Physik, Giessenbachstrasse, PF 1312, 85741 Garching, Germany*

[c] *Department of Physics, San Diego State University, 5500 Campanile Drive, San Diego, California 92182, USA*

Abstract

The cooling of a compact star depends very sensitively on the state of matter at supranuclear densities, which essentially controls the neutrino emission, as well as on the structure of the stellar outer layers which control the photon emission. Open issues concern the hyperon population, the presence of meson condensates, superfluidity and superconductivity, and the transition of confined hadronic matter to quark matter. This paper describes these issues and presents cooling calculations based on a broad collection of equations of state for neutron star matter and strange matter. These results are tested against the body of observed cooling data.

Key words: Nuclear matter, Quark Matter, Equation of state, Neutron stars, Cooling
PACS: 97.10.Cv, 97.60.Jd, 26.60+c, 12.38.Mh

1 Introduction

Cooling simulations, confronted with soft X-ray, extreme UV, UV and optical observations of the thermal photon flux emitted from the surfaces of neutron stars, provide most valuable information about the physical processes

Email addresses: page@astroscu.unam.mx (Dany Page[1]), urme@xray.mpe.mpg.de (Ulrich Geppert), fweber@sciences.sdsu.edu (Fridolin Weber[2]).

[1] D. P. work is partially supported by a grant from UNAM-DGAPA, #IN112502
[2] F. W. research was supported by an award from Research Corporation.

operating in the interior of these objects. The predominant cooling mechanism of hot (internal temperatures $T \gtrsim 10^{10}$ K) newly formed neutron stars is neutrino emission, with an initial cooling time scale of seconds. Neutrino cooling still dominates for at least the first thousand years, and typically for much longer in slow (standard) cooling scenarios. Photon emission eventually overtakes neutrinos when the internal temperature has sufficiently dropped. Being sensitive to the adopted nuclear equation of state (EOS), the stellar mass, the assumed magnetic field strength, superfluidity, meson condensates, and the possible presence of color-superconducting quark matter, theoretical cooling calculations serve as a principal window on the properties of superdense hadronic matter and neutron star structure. The thermal evolution of neutron stars also yields information about such temperature-sensitive properties as transport coefficients, crust solidification, and internal pulsar heating mechanisms.

We will present here an overview of the current status of neutron star cooling calculations tested against the steadily growing body of observed cooling data on neutron stars. The reader can also find a complementary approach in Ref. [1]. Space limitation forbid us to dwell into the discussion of observational data and we refer the reader to Ref. [2] for a recent compilation and to two recent observational reviews [3,4] to get a flavor of the difficulties involved in the analysis and interpretation of the data.

The paper is organized as follows. In § 2 we introduce the basic equations and the physics input that governs neutron star cooling. Some simple analytical solutions to the cooling equations are presented in § 3. The minimal cooling paradigm, which assumes that no enhanced neutrino emission is allowed in neutron stars, is presented in § 4. In § 5 we discuss enhanced neutron star cooling via the direct Urca process, meson condensates, and quarks. The cooling behavior of compact stars made of absolutely stable strange quark matter is explored in § 6. The impact of magnetic fields on cooling and heating mechanisms is discussed in § 7 and § 8, respectively while § 9 considers cooling neutron stars in transiently accreting binary systems. Conclusions are offered in § 10.

2 Basic Equations and Physics Input

The basic features of the cooling of a neutron star are easily grasped by simply considering the energy balance equation for the star. In its Newtonian formulation this equation reads

$$\frac{dE_{\rm th}}{dt} = C_{\rm v}\frac{dT}{dt} = -L_\nu - L_\gamma + H\,, \tag{1}$$

where $E_{\rm th}$ is the thermal energy content of the star, T its internal temperature, and $C_{\rm v}$ its total specific heat. The energy sinks are the total neutrino luminosity L_ν, described in § 2.2, and the surface photon luminosity L_γ, discussed in § 2.6. The source term H includes all possible "heating mechanisms" which, for instance, convert magnetic or rotational energy into heat as summarized in § 8. Some simple analytical solutions to Eq. (1) will be presented in § 3.

The dominant contributions to $C_{\rm v}$ come from the core, constituting more than 90% of the total volume, whose constituents are quantum liquids of leptons, baryons, mesons, and possibly deconfined quarks at the highest densities. When baryons, and quarks, become paired, as briefly described in § 2.3, their contribution to $C_{\rm v}$ is strongly suppressed at temperatures $T \ll T_{\rm c}$ ($T_{\rm c}$ being the corresponding critical temperature). The crustal contribution is in principle dominated by the free neutrons of the inner crust but, since these are certainly extensively paired, practically only the nuclear lattice and electrons contribute. Extensive baryon, and quark, pairing can thus significantly reduce $C_{\rm v}$, but by at most a factor of order ten since the leptons do not pair.

All results presented in this chapter were obtained with numerical codes which exactly solve both the energy balance and the heat transport equations in their General Relativistic forms (see, e.g., [2,5]). Since the density and chemical composition of the star, after the proto-neutron star phase, do not change with time, the Tolman-Oppenheimer-Volkoff equation of hydrostatic equilibrium is solved initially, for a given EOS, and only the thermal equations are evolved with time. The outermost, low density, layers of the star do see their structure evolve during the cooling and they are hence treated separately as an envelope which is the outer boundary condition and is described in § 2.6.

2.1 The Equation of State (EOS)

The cross section of a neutron star can be split roughly into three, possibly four, distinct regimes. The first regime is the star's outer crust, which consists of a lattice of atomic nuclei and a Fermi gas of relativistic, degenerate electrons. The second regime, known as the inner crust and where free neutrons appear, extends from neutron drip density, $\sim 4 - 8 \times 10^{11}$ g cm^{-3}, to a transition density of about 2×10^{14} g cm^{-3}. Beyond that density one enters the star's third regime, its core matter where all atomic nuclei have dissolved into their constituents, protons and neutrons. Furthermore, because of the high Fermi pressure, the inner core may be expected to contain baryon resonances, boson condensates, hyperons, or/and a mixture of deconfined up, down and strange quarks [6,7]. The EOS of the outer and inner crust is rather well known. This is very different for the EOS of the star's core which is only very poorly understood. Models derived for it fall into non-relativistic EOS and relativistic,

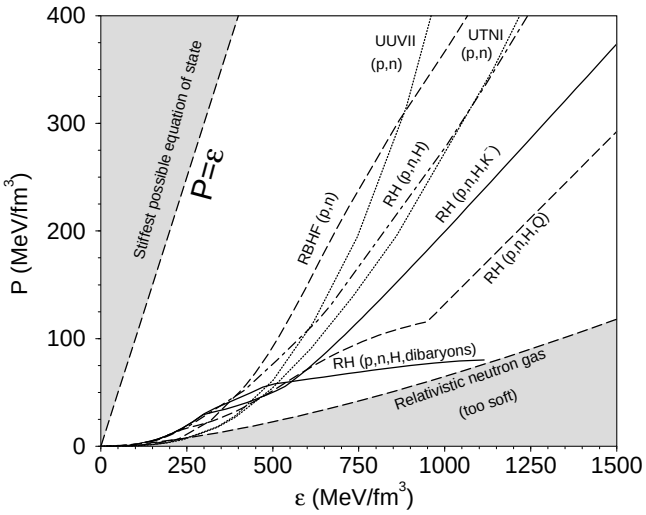

Fig. 1. Models for the EOS of high-density neutron star matter computed for different compositions and many-body techniques. (p,n denote protons and neutrons; H, K^-, Q stand for hyperons, K^- condensate, and quarks, respectively.)

field theoretical ones.

The most frequently used non-relativistic models for the EOS are based on the hole-line expansion (Brueckner theory), the coupled cluster method, self-consistent Green functions, the variational approach (Monte Carlo techniques), the semi-classical Thomas-Fermi method, and the density functional approach based on Skyrme effective interactions (for an overview of these methods and additional references, see for instance Refs. [8–10]). The forces between hadrons are described in terms of phenomenological nucleon-nucleon interactions, possibly supplemented with three-nucleon interactions to achieve a better agreement with the binding energy of nuclear matter at the empirical saturation density. Figure 1 shows two sample models for the EOS of neutron star matter (protons and neutrons only) which are obtained from variational calculations based on the Urbana V_{14} two-nucleon interaction supplemented with the three-body interactions UVII (left curve) and TNI (right curve) [11].

Relativistic, field-theoretical approaches to the EOS are based on model Lagrangians which generally describe baryons as Dirac particles interacting via the exchange of mesons. The most important mesons are the σ and the ω, which are responsible for nuclear binding, while the ρ meson is required to obtain the correct value for the empirical symmetry energy. Nonlinear σ terms need to be included at the mean-field (relativistic Hartree, RH) level in order to obtain the empirical incompressibility of nuclear matter [6]. Such terms are not necessary if the field equations are solved for the relativistic Brueckner-Hartree-Fock (RBHF) approximation [7]. In contrast to RH, where the parameters of the theory are adjusted to the properties of infinite nuclear matter, the RBHF method makes use of one-boson-exchange potentials whose parameters are adjusted to the properties of the deuteron and to the nucleon-nucleon

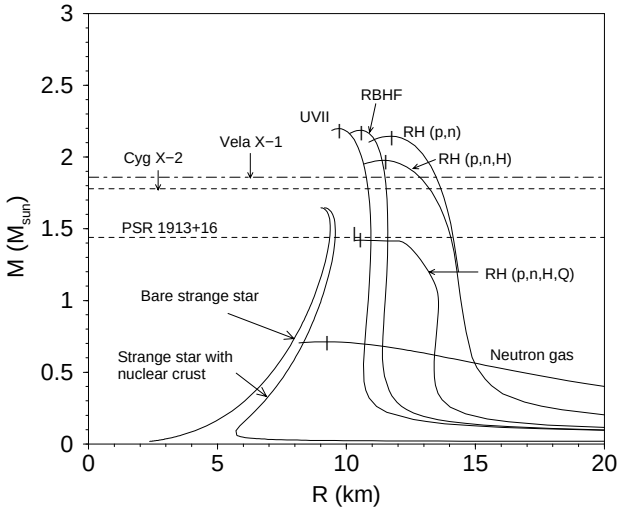

Fig. 2. Neutron star mass versus radius for different EOSs. The horizontal lines refer to the masses of Vela X-1 ($1.88 \pm 0.13\, M_\odot$ if the inclination angle of the system is $i = 90^o$; an inclination angle of $i = 70^o$ increases the star's mass to $2.27 \pm 0.17\, M_\odot$ [15]), Cyg X-2 ($1.78 \pm 0.23\, M_\odot$ [16]; Titarchuck and Shaposhnikov obtain for Cyg X-2 a mass of $1.44 \pm 0.06\, M_\odot$ [17]), and PSR 1913+16 ($1.4408 \pm 0.0003\, M_\odot$) [18] (in all three cases quoted mass uncertainties are 1σ).

scattering data. Figure 1 shows several sample EOSs computed for RH and RBHF, assuming different particle compositions of neutron star matter [7]. Finally we mention that in recent years a new class of effective field theories was developed which treat the meson-nucleon couplings as density dependent. These field theories provide a very good description of the properties of nuclear matter, atomic nuclei as well as neutron stars [12–14].

In Figure 2 we show the mass-radius relationships of neutron stars for different EOSs: it illustrates the well-known fact that this relationship is very sensitive to the underlying model for the EOS.

Phase transitions to boson condensates, hyperonic matter, or quark matter, soften the EOS, hence reducing both the stars gravitational mass and radius and resulting in a smaller maximum mass sustainable by the EOS. A generically different mass-radius relationship is obtained for stars made of absolutely stable strange quark matter (strange stars). For them $M \propto R^3$, which is only significantly modified if M is close to the mass peak. As pointed out in [19], strange stars can carry a solid nuclear crust whose density at its base is strictly limited by neutron drip. This is made possible by the displacement of electrons at the surface of strange matter, which leads to a strong electric dipole layer there. The associated electric field is so strong that it holds open a gap between the nuclear crust and quark matter, preventing the conversion of the crust into the hypothetical lower-lying ground state of strange matter. Obviously, free neutrons, being electrically charge neutral, cannot exist in the crust because they do not feel the Coulomb barrier and thus would

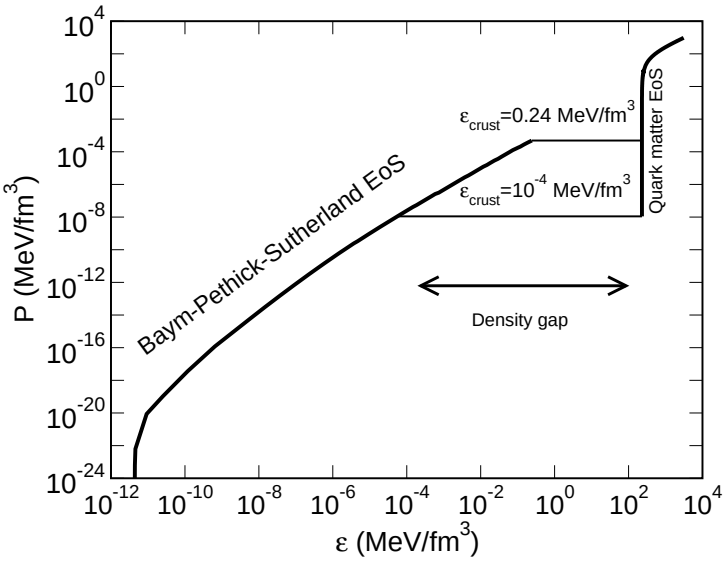

Fig. 3. EOS of strange quark matter surrounded by nuclear matter. The maximal possible nuclear matter density is determined by neutron drip which occurs at $\epsilon_{\rm crust} = 0.24$ MeV fm^{-3} (4.3×10^{11} g cm^{-3}). Any nuclear density that is smaller than that is possible. As an example, we show the EOS for a sample density of $\epsilon_{\rm crust} = 10^{-4}$ MeV fm^{-3} (10^8 g cm^{-3}).

gravitate toward the strange quark matter core where they are converted, by hypothesis, into strange matter. Consequently, the density at the base of the crust will always be smaller than neutron drip. The situation is graphically illustrated in Figure 3 which shows the EOS of a strange star [7,20] carrying a nuclear crust. Since the crust is bound to the quark matter core by gravity rather than confinement, the mass-radius relationship of strange stars with a nuclear crust is intermediate between the one of bare strange stars and of purely gravitationally bound neutron stars, as shown in Figure 2.

2.2 Neutrino Processes

As already mentioned in the introduction, neutron stars are born with temperatures in excess of 10^{10} K. The dominating cooling mechanism of such objects, for $\sim 10^4 - 10^5$ years after birth, is neutrino emission from the interior. After that, cooling via photon emission from the star's surface takes over. Tables 1 and 2 summarize the dominant neutrino emitting processes together with their efficiency for neutron star cooling and we now briefly describe the most important ones. The reader is referred to Refs. [7,21–23] for more details. We will nevertheless comment in § 2.5 on minor neutrino emission processes which may become important in cases where all the dominant ones, as discussed in § 2.3, are suppressed by pairing.

Direct Urca Processes. The beta decay and electron capture processes

Table 1
Dominant neutrino emitting processes in neutron star cores, in absence of hyperons[a] and quarks[b].

Name	Process[c]	Emissivity[d] (erg cm^{-3} s^{-1})	
Modified Urca cycle (neutron branch)	$n+n \to n+p+e^- +\bar{\nu}_e$ $n+p+e^- \to n+n+\nu_e$	$\sim 2{\times}10^{21}\, R\, T_9^8$	Slow
Modified Urca cycle (proton branch)	$p+n \to p+p+e^- +\bar{\nu}_e$ $p+p+e^- \to p+n+\nu_e$	$\sim 10^{21}\, R\, T_9^8$	Slow
Bremsstrahlung	$n+n \to n+n+\nu+\bar{\nu}$ $n+p \to n+p+\nu+\bar{\nu}$ $p+p \to p+p+\nu+\bar{\nu}$	$\sim 10^{19}\, R\, T_9^8$	Slow
Cooper pair formations	$n+n \to [nn]+\nu+\bar{\nu}$ $p+p \to [pp]+\nu+\bar{\nu}$	$\sim 5{\times}10^{21}\, R\, T_9^7$ $\sim 5{\times}10^{19}\, R\, T_9^7$	Medium
Direct Urca cycle	$n \to p+e^- +\bar{\nu}_e$ $p+e^- \to n+\nu_e$	$\sim 10^{27}\, R\, T_9^6$	Fast
π^- condensate	$n+<\pi^->\to n+e^- +\bar{\nu}_e$	$\sim 10^{26}\, R\, T_9^6$	Fast
K^- condensate	$n+<K^->\to n+e^- +\bar{\nu}_e$	$\sim 10^{25}\, R\, T_9^6$	Fast

[a] In the presence of hyperons, most processes listed here have corresponding ones with hyperons replacing nucleons.
[b] See Table 2 for quark processes.
[c] Where μ^- are present, all processes involving e^- have a corresponding one with μ^-, ν_μ, and $\bar{\nu}_\mu$ replacing e^-, ν_e, and $\bar{\nu}_e$, respectively.
[d] Quoted emissivities are only indicative: each process has its specific dependences on medium and particle densities, effective masses, plus medium effect corrections, for which we refer the reader to Refs. [7,21–23]; the many R factors are the respective temperature dependent control functions which take into account the effects of pairing as discussed in § 2.3 and detailed in Ref. [22].

among nucleons, $n \to p+e^- +\bar{\nu}_e$ and $p+e^- \to n+\nu_e$, also known as nucleon direct Urca process (or cycle), are only possible in neutron stars if the proton fraction exceeds a critical threshold [24]. Otherwise energy and momentum can not be conserved simultaneously for these reactions. For a neutron star made up of only neutrons, protons and electrons, the critical proton fraction is around 11%. This follows readily from $\mathbf{k}_{F_n} = \mathbf{k}_{F_p} + \mathbf{k}_{F_e}$ combined with the condition of electric charge neutrality of neutron star matter. The triangle inequality then requires for the magnitudes of the particle Fermi momenta $k_{F_n} \leq k_{F_p} + k_{F_e}$, and charge neutrality constrains them to $k_{F_p} = k_{F_e}$. Substituting $k_{F_p} = k_{F_e}$ into the triangle inequality leads to $k_{F_n} \leq 2k_{F_p}$ so that $n_n \leq 8n_p$ for the number densities of neutrons and protons. Expressed as a fraction of the system's total baryon number density, $n \equiv n_p + n_n$, one thus arrives at

$n_p/n > 1/9 \simeq 0.11$ as quoted above. Medium effects and interactions among the particles modify this value only slightly but the presence of muons raises it to about 0.15. Hyperons, which may exist in neutron star matter rather abundantly, produce neutrinos via the direct Urca process $\Sigma^- \to \Lambda + e^- + \bar{\nu}_e$ with $\Lambda + e^- \to \Sigma^- + \nu_e$ and similar ones involving hyperons and nucleons simultaneously [25]. Which of these processes dominates the cooling depends on the details of the star's composition, but in most cases the nucleon direct Urca process is more efficient than the ones involving hyperons [26,27].

Meson Condensate Urca Processes. The pion or kaon meson fields may develop condensates in dense neutron star matter. These condensates would have two important effects on neutron stars. Firstly, they would soften the EOS above the critical density for onset of condensation, which reduces the maximal possible neutron star mass. Secondly, since the condensate, $<\pi^->$ or $<K^->$, can absorb as little or as much momentum as required by the scattering processes $n+ <\pi^-> \to n + e^- + \bar{\nu}_e$ or $n+ <K^-> \to n + e^- + \bar{\nu}_e$, the resulting neutrino emissivities of meson-condensed matter [28–30], even though not as high as the ones of the direct Urca processes (see Table 1), still lead to fast cooling [31–33]. Since the K^--condensate process involves strangeness change it is less efficient than the π^--condensate process, roughly by a factor $\sin^2\theta_C \simeq 1/20$ (θ_C being the Cabibbo angle). However, medium effects can reduce the π^--condensate process by about one order of magnitude and make it comparable to the K^--condensate one [34]. Estimates predict the onset of charged pion condensation at a density $n_{\rm cr}^{\pi} \sim 2n_0$ ($n_0 = 0.16$ fm^{-3} being the empirical nuclear matter density). However, this value is very sensitive to the strength of the effective nucleon particle-hole repulsion in the isospin-1, spin-1 channel, which tends to suppress the π-condensation mechanism and may push $n_{\rm cr}^{\pi}$ to much higher values. Similarly, depending on the nuclear model, the threshold density for the onset of kaon condensation, $n_{\rm cr}^{K}$, is at least of the order of $4n_0$ [35].

Modified Urca Processes. In absence of hyperons or meson condensates, or in case the proton fraction is below threshold, none of the above described Urca processes is possible. In this case, the dominant neutrino emission process is a second order process, variant of the direct Urca process, called modified Urca process [36,37], in which a bystander neutron or proton participates to allow momentum conservation (see Table 1). Since this modified Urca process involves 5 degenerate fermions, instead of three for the direct Urca and meson Urca processes, its efficiency is reduced, simply by phase space limitation, by a factor of order $(T/T_{\rm F})^2$. This reduction, for $T_{\rm F} \sim 100$ MeV and $T = 0.1$ MeV $\simeq 10^9$ K, amounts to about 6 order of magnitude (!) and an overall temperature dependence T^8 instead of T^6. It is certainly the dominant process for not too high densities in absence of pairing, and is the essence of the old "Standard Cooling Scenario". However, in presence of pairing, neutrino emission by the constant formation of Cooper pairs, see § 2.3, most probably dominates over

Table 2
Dominant neutrino emitting processes in deconfined quark matter.

Name	Process[a]	Emissivity[b] (erg cm^{-3} s^{-1})	Efficiency
Direct Urca cycle (ud branch)	$u + e^- \to d + \nu_e$ $d \to u + e^- + \bar{\nu}_e$	$\sim 10^{26}\, R\, T_9^6$	Fast
Direct Urca cycle (us branch)	$u + e^- \to s + \nu_e$ $s \to u + e^- + \bar{\nu}_e$	$\sim 10^{25}\, R\, T_9^6$	Fast
Modified Urca cycle (ud branch)	$Q + u + e^- \to Q + d + \nu_e$ $Q + d \to Q + u + e^- + \bar{\nu}_e$	$\sim 10^{21}\, R\, T_9^8$	Slow
Modified Urca cycle (us branch)	$Q + u + e^- \to Q + s + \nu_e$ $Q + s \to Q + u + e^- \bar{\nu}_e$	$\sim 10^{20}\, R\, T_9^8$	Slow
Bremsstrahlungs	$Q_1 + Q_2 \to Q_1 + Q_2 + \nu + \bar{\nu}$	$\sim 10^{19}\, R\, T_9^8$	Slow
Cooper pair formations	$u + u \to [uu] + \nu + \bar{\nu}$ $d + d \to [dd] + \nu + \bar{\nu}$ $s + s \to [ss] + \nu + \bar{\nu}$	$\sim 2.5{\times}10^{20}\, R\, T_9^7$ $\sim 1.5{\times}10^{21}\, R\, T_9^7$ $\sim 1.5{\times}10^{21}\, R\, T_9^7$	Medium

[a] Muons are never present in quark matter. In case the quark matter is negatively charged e^+ are present instead of e^- and processes involving e^- are replaced by similar ones involving e^+.
[b] Quoted emissivities are only indicative: each process has its specific dependences on medium and particle densities, strange quark mass m_s, and color coupling constant α_c, see Ref. [7,41,42] for more details; the many R factors are the respective control functions which take into account the effects of pairing as discussed in § 2.3.

the modified Urca process.

Since the modified Urca process involves a strong interaction for the momentum exchange between the neutrino emitting nucleon and the bystander one, it is prone to medium corrections which seem to result in a reduction of emissivity (see. e.g., [38,39]). However, softening of the pion mode, which eventually leads to π^--condensation, do results in a very strong enhancement of the emissivity when the density approaches $n_{\rm cr}^{\pi}$, and gives a smooth transition from the modified Urca process toward the π^--condensate process through a *medium-modified-Urca* process ("MMU" process [23,40]).

The Quark Urca Processes. The neutrino emission processes in non-superconducting quark matter [41] can be divided into slow and fast ones, in complete analogy to the nucleon processes discussed above, and the dominant processes are listed in Table 2. The fast quark direct Urca processes $d \to u + e^- + \bar{\nu}_e$ and $s \to u + e^- + \bar{\nu}_e$ are only possible if the Fermi momenta of quarks and electrons obey the triangle inequalities associated with these reactions, which are $k_{F_d} < k_{F_u} + k_{F_e}$ and $k_{F_s} < k_{F_u} + k_{F_e}$. If the electron Fermi momentum, k_{F_e},

in quark matter is too small for the quark triangle inequalities to be fulfilled, a bystander quark is needed to ensure energy and momentum conservation in the scattering process. This latter case is referred to as quark modified Urca process. The emissivities associated with the quark modified Urca processes are considerably smaller than those of the direct Urca processes because of the different phase spaces associated with two-quark scattering and quark decay. In the extreme case when the electron fraction vanishes entirely in quark matter, both the quark direct and the quark modified Urca processes become unimportant. The neutrino emission from the star is then dominated by bremsstrahlung processes, $Q_1 + Q_2 \rightarrow Q_1 + Q_2 + \nu + \bar{\nu}$, where Q_1 and Q_2 denote any pair of quark flavors. In this case, stellar cooling proceeds rather slowly.

Notice that non-Fermi liquid corrections lead to an enhancement of the emissivities compared to the results of [41] and Table 2, which for the direct Urca is of order $(\log(mc^2/k_BT))^2$, with $mc^2 \sim 400$ MeV [43]. However this effect has not yet been incorporated in numerical calculations and is balanced by a similar increase in the specific heat so that the net result of non-Fermi liquid effect is not expected to be very large [43].

2.3 Pairing

Pairing will unavoidably occur in a degenerate Fermi system in case there is *any* attractive interaction between the particles. In case of the baryons, and quarks, in the neutron star interior there are many candidates for channels of attractive interactions, and the real question is rather what is the critical temperature $T_{\rm c}$ at which pairing occurs? Calculation of $T_{\rm c}$ are notoriously difficult and results often highly uncertain. We refer the reader to [44,45] for detailed reviews. With respect to leptons, there is no obvious attractive interaction which could lead to pairing with a $T_{\rm c}$ of significant value.

In the case of nucleons, at low Fermi momenta, pairing is predicted to occur in the $^1S_0$ angular momentum state while at larger momenta neutrons are possibly paired in the $^3P_2 - {}^3F_2$ state (the mixing being due to the tensor interaction). In the case of the neutron $^1S_0$ pairing, which occurs at densities corresponding to the crust and, possibly, the outermost part of the core, much efforts have been invested in its study and calculations are converging with time when more and more sophisticated many-body models are used. In the case of the proton $^1S_0$ pairing the situation is more delicate since it occurs at densities (in the outer core) where protons are mixed, to a small amount, with neutrons. Predictions for $T_{\rm c}$ span a much wider range than in the case of the neutron $^1S_0$ gap. Whether or not neutrons pair in the $^3P_2 - {}^3F_2$ channel is still uncertain, since even the best available models for the nucleon-nucleon

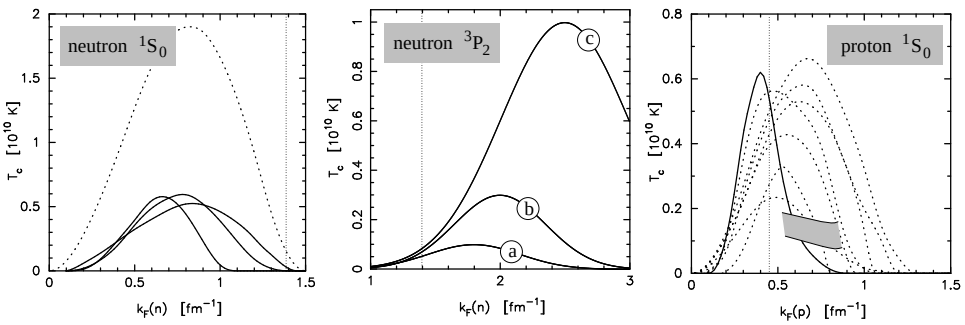

Fig. 4. Predictions for the nucleon pairing $T_{\rm c}$. Left panel: neutron $^1S_0$ pairing; three most recent calculations (continuous lines) which include medium polarization effects while the dotted line shows the result in case these effects are neglected. Right panel: same for protons; no polarization effects are taken into account except for the continuous curve; the shaded area shows the range of expected $T_{\rm c}$'s when polarization is taken into account, according to the estimates of [50]. Central panel: neutron $^3P_2$ pairing; three typical results, none including polarization effects, illustrating the possible range according to [46]. See [2] for details and references.

interaction fail to reproduce the measured $^3P_2$ phase shift *in vacuum* [46]. Moreover, the results of [47], which consider polarization contributions to the effective interaction, indicate that this gap may be vanishingly small. A set of representatives predictions for the nucleon gaps are shown in Figure 4.

The enormous impact of pairing on the cooling comes directly from the appearance of the energy gap Δ at the Fermi surface which leads to a suppression of all processes involving single particle excitations of the paired species. When $T \ll T_{\rm c}$ the suppression is of the order of $e^{-\Delta/k_{\rm B}T}$ and hence dramatic. The suppression depends on the temperature dependence of Δ and the details of the phase space involved in each specific process. In numerical calculations it is introduced as a control function. For the specific heat one has

$$c_{\rm v}(T) \longrightarrow c_{\rm v}^{\rm paired}(T) = R_c(T/T_{\rm c}) \times c_{\rm v}^{\rm normal}(T)\,, \tag{2}$$

and the control functions have been calculated for both $^1S_0$ and $^3P_2$ pairing in [48]. For neutrino processes there is a long family of control functions for all processes which must also consider which of the participating baryons are paired. As for $c_{\rm v}$ one uses

$$\epsilon_\nu(T) \longrightarrow \epsilon_\nu^{\rm paired}(T) = R_\nu(T/T_{\rm c}) \times \epsilon_\nu^{\rm normal}(T)\,, \tag{3}$$

and the R_ν's for many processes can be found in [49]. We plot in Figure 5 several examples of control functions.

It is important to notice that the gap Δ is actually a function of the particle momentum, $\Delta = \Delta(\mathbf{k})$. For $^1S_0$ pairing it is isotropic, i.e., $\Delta = \Delta(k)$, but for

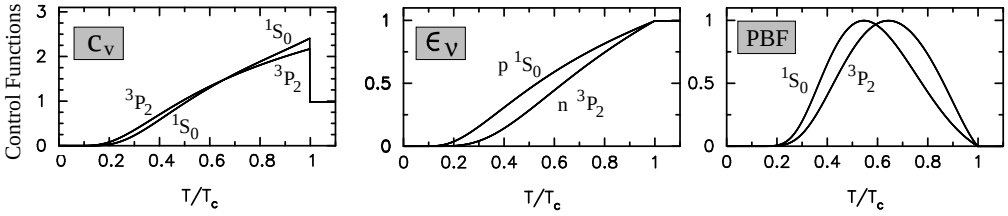

Fig. 5. Control functions for $c_{\rm v}$ (left panel), Eq. (2), ϵ_ν of the neutron branch of the modified Urca process for the case of either neutron or proton pairing (central panel), Eq. (3), and the PBF process, Eq. (5) (right panel).

$^3P_2 - ^3F_2$ pairing the angular dependence of $\Delta(\mathbf{k})$ is complicated. In this latter case many phases, with distinct angular dependences of $\Delta(\mathbf{k})$ are possible ([51] found there are *at least* 13 of them) and for several of them $\Delta(\mathbf{k})$ has nodes at some points or along some lines on the Fermi surface. The control functions plotted in Figure 5 assume nodeless gaps, but in cases of 1D nodes $R \sim (T/T_c)^2$, while for 2D nodes $R \sim T/T_c$, at $T \ll T_c$ instead of a Boltzmann-like suppression.

Cooper Pair Breaking and Formation (PBF) Processes. Besides the above described, and well known, suppressing effects on the specific heat and neutrino emissivities, the onset of pairing also opens new channels for neutrino emission. The superfluid or superconducting condensate is in thermal equilibrium with the single particle ("broken pairs") excitations and there is continuous formation and breaking of Cooper pairs, which are very intense at temperatures slightly below $T_{\rm c}$. The formation of a Cooper pair liberates an energy which can be taken away by a ν-$\overline{\nu}$ pair [52,53]

$$X + X \longrightarrow [XX] + \nu + \overline{\nu} \tag{4}$$

where $[XX]$ denotes a Cooper pair of particles X (X stands for neutrons, protons, hyperons, quarks, etc.). As an example, the emissivity for neutron $^3P_2$ pairing is [49] [3]

$$q_\nu^{n,\,^3P_2} = 8.6 \times 10^{21} \left(\frac{n_{\rm n}}{n_0}\right)^{1/3} \left(\frac{m_n^*}{m_n}\right) \times R_{^3P_2}(T/T_{\rm c}) \left(\frac{T}{10^9\ {\rm K}}\right)^7 , \tag{5}$$

where the control function R is plotted in the right panel of Figure 5: the process turns on at $T = T_{\rm c}$, with an increasing efficiency when T decreases, since the energy of the emitted neutrinos is determined by the gap's size which grows with decreasing temperature just below $T_{\rm c}$, and is eventually exponentially suppressed when $T \ll T_{\rm c}$ as pair breaking is frozen because $k_{\rm B}T \ll \Delta$. This process can be seen as a bremsstrahlung with a very strong

[3] Our control function R differs from the F of Eq. (236) in [49] in that it is normalized to have a maximum value of one.

correlation in the final state and referring to Tables 1 and 2, one sees that it is much more efficient that the simple bremsstrahlung and it can even dominate over the standard modified Urca process. This process, which is as standard as the modified Urca process, is an essential ingredient of the Minimal Cooling Paradigm described in § 4. Analogous processes occur for all cases of pairing: neutron, proton, hyperons, and quarks [42].

2.4 Color-Superconductivity of Quark Matter

Already several decades ago it had been suggested that the attractive force among quarks may cause them to form Cooper pairs [54,55]. Originally the gap was estimated to be around $\Delta = 0.4$ MeV [55]. Recently, however, it was discovered that the condensation patterns of quark matter are much more complex than originally thought [56,57]. This has its origin in the fact that quarks come in different colors, different flavors, and different masses. Moreover, bulk matter is neutral with respect to both electric and color charge, and is in chemical equilibration under the weak interaction processes that turn one quark flavor into another. Depending on density and temperature, quarks may thus condense in one of the following pairing schemes. At asymptotic densities the ground state of (3-flavor) QCD with a vanishing strange quark mass is the color-flavor locked (CFL) phase in which all three quark flavors participate symmetrically. This phase has been shown to be electrically neutral without any need for electrons for a significant range of chemical potentials and strange quark masses [58]. In the opposite limit where the strange quark mass m_s is large enough that strange quarks can be ignored, then up and down quarks may pair in the 2-flavor superconducting (2SC) phase. Other possible condensation patterns are CFL-K^0, CFL-K^+ and CFL-$\pi^{0,-}$, gCFL (gapless CFL phase), 1SC (single-flavor-pairing), CSL (color-spin locked phase), and the LOFF (Larkin, Ovchinnikov, Fulde, and Ferrell) crystalline pairing phase, depending on the quark flavor densities, the quark chemical potential μ_q, and electric charge density. For chemical potentials that are of astrophysical interest, $\mu_q < 1000$ MeV, the color gap is between 50 and 100 MeV, which has a significant impact on stellar cooling by neutrino emission.

2.5 Comments on minor neutrino emission processes

The neutrino processes described in § 2.2 are usually the dominant ones but in particular cases some minor processes may become important.

During the first few years of the life of the compact star the surface temperature is entirely controlled by neutrino emission in its upper layers and is independent of what is happening in the core [29,59–61]. In this case the

dominant process is plasmon decay (see, e.g., [49]) which very efficiently cools every layer in the the outer crust until the temperature T drops below $\hbar\Omega_P/k_B$ (Ω_P being the electron plasma frequency in the layer) and plasmons are exponentially suppressed. As a result, the effective temperature is $T_e \simeq 2.5 \times 10^6$ K (in case of a heavy element envelope) for all young compact stars independently of the core temperature, as can be seen from the numerical results presented in Figure 11. Later on the crust will cool by neutrino emission from the electron-ion and electron-electron bremsstrahlung processes [49,62] and the PBF process from the neutron $^1S_0$ superfluid in the inner crust. This is not very important at present time since there are no data about such young compact stars, but may become essential in case a compact object is detected within the remnant of the supernova SN 1987A.

For middle-age stars, in case all processes described in § 2.2 and § 2.3 are strongly suppressed by very large gaps, neutrino emission from the crust, as described in the previous paragraph, is important. Despite of the small amount of mass present in the crust, omission of its neutrino emission may then lead to erroneous results, i.e., too warm stars. All numerical results presented in this paper of course include these processes.

2.6 The Surface Photon Luminosity and the Envelope

The photon luminosity L_γ is traditionally expressed as

$$L_\gamma = 4\pi R^2 \cdot \sigma_{\rm SB} T_{\rm e}^4 \,, \tag{6}$$

which *defines* the effective temperature $T_{\rm e}$ ($\sigma_{\rm SB}$ being the Stefan-Boltzmann constant and R the stellar radius). The quantities L, R, and $T_{\rm e}$ are local quantities as measured by an observer at the stellar surface. An external observer "at infinity" will measure these quantities red-shifted, i.e., $L_\infty = e^{2\phi} L_\gamma$, $T_\infty = e^{\phi} T_{\rm e}$, and $R_\infty = e^{-\phi} R$, where $e^{2\phi} \equiv g_{00}$ is the time component of the metric and is related to the red-shift z by $e^{-\phi} = 1 + z$, so that

$$L_\infty = 4\pi R_\infty^2 \cdot \sigma_{\rm SB} T_\infty^4 \,. \tag{7}$$

The luminosity L_γ, or L_∞, is the main output of a cooling calculation, and it can equally well be expressed in terms of $T_{\rm e}$ or T_∞.

Numerical simulations calculate the time evolution of the internal temperature $T = T(\rho, t)$ and luminosity $L = L(\rho, t)$ profiles (viewed as functions of the density ρ instead of the radius r) up to an outer boundary $\rho_{\rm b}$. This boundary is chosen such that at this point the diffusive luminosity $L(\rho_{\rm b})$ is equal to the photon luminosity at the surface, i.e., $L(\rho_{\rm b}) \equiv L_\gamma$, and an envelope model is

glued as an outer boundary condition. Typically $\rho_{\rm b}$ is taken as 10^{10} g cm^{-3} and the envelope is thus a thin layer, of the order of a hundred meters thick, which is treated in the plane parallel approximation. Assuming that the thermal relaxation time-scale of the envelope is much shorter than the stellar evolution time-scale, and that neutrino emission in the envelope is negligible, hydrostatic equilibrium and heat transport reduce to ordinary differential equations which, with the appropriate physical input, are easily solved. The result is a surface temperature $T_{\rm s} \equiv T_{\rm e}$ for each given $T_{\rm b} \equiv T(\rho_{\rm b})$. It is usually called a $T_{\rm b} - T_{\rm s}$ or $T_{\rm b} - T_{\rm e}$ relationship. Through Eq. (6), this gives us a relationship between $L(\rho_{\rm b}) \equiv L_\gamma$ and $T(\rho_{\rm b})$ which is the outer boundary condition for the cooling code.

It has been shown in Refs. [63,64] that $T_{\rm e}$ is actually controlled by a "sensitivity layer", where electrons become partially degenerate and ions are in the liquid phase. At higher densities the highly degenerate electrons are extremely efficient in transporting heat while at lower densities photons take over and are also very efficient. The density at which the sensitivity layer is located increases with increasing $T_{\rm b}$. This sensitivity layer is hence a throttle and, once heat has passed through it, it can freely flow to the surface and be radiated. The layers at densities below the sensitivity layer have no effect at all on the thermal evolution of the star, since they are unable to alter the heat flow, but the outermost layer, the photosphere, is of course of upmost observational importance since it is there that the energy distribution of the emerging flux, i.e., the observable spectrum, is determined.

Gluing an envelope to an interior solution is a standard technique in stellar evolution codes. For neutron stars it has two extra advantages: it relieves us from solving for hydrostatic equilibrium in the interior, since matter there is degenerate, and, most importantly, it allows one to easily include magnetic field effects. The magnetic field slightly enhances heat transport along it but strongly suppresses it in the perpendicular direction, resulting in a highly non uniform surface temperature [65]. Assuming that magnetic field effects on heat transport are negligible at $\rho > \rho_{\rm b}$ one keeps spherical symmetry in the interior and thus has a unique $T_{\rm b}$ at $\rho_{\rm b}$. For this given uniform $T_{\rm b}$ one can piece together a set of envelope calculations for the various field strengths and orientations along the stellar surface, corresponding to the assumed magnetic field structure, and thus obtain a non uniform surface temperature distribution $T_s(\theta, \phi)$, in spherical coordinates (θ, ϕ) [66,67]. The effective temperature is simply obtained by averaging the locally emerging photon flux $F_\gamma(\theta, \phi) \equiv \sigma_{\rm SB}\, T_{\rm s}^4(\theta, \phi)$ over the whole stellar surface

$$T_{\rm e}^4 \equiv \frac{1}{4\pi} \iint T_{\rm s}^4(\theta, \phi)\ \sin\theta\, d\theta d\phi \tag{8}$$

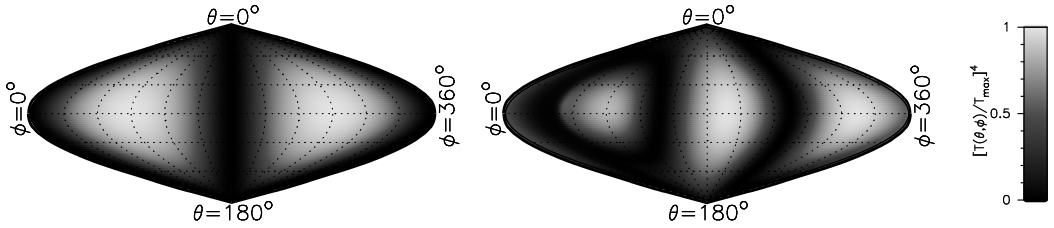

Fig. 6. Two examples of surface temperature distributions induced by the magnetic field, in an area preserving projection of the neutron star surface (grey shading, shown on the right scale, follows the surface flux instead of the temperature). Left panel assumes a dipolar field, with strength 1.2×10^{12} G at the pole located at $(\theta, \phi) = (90^o, 90^o)$: for a core temperature of 4.05×10^7 K it gives $T_{\rm e} = 5.43 \times 10^5$ K (see Eq. 8) while the maximum and minimal surface temperatures, at the magnetic poles and along the magnetic equator, respectively, are $T_{\rm max} = 6.70 \times 10^5$ K and $T_{\rm min} = 1.4 \times 10^5$ K. The right panels shows the effect the same dipolar field to which a quadrupolar component has been added: this results in $T_{\rm e} = 5.31 \times 10^5$ K. This particular latter case allows one to reproduce the observed ROSAT X-ray pulse profile of Geminga (see Figure 6 in [67]) which shows a single very broad pulse while a purely dipolar field would result in a double pulse profile (assuming the observer is in the direction $\theta \simeq 90^o$ and emission is isotropic blackbody). Finally, in absence of magnetic field, the same internal temperature would result in $T_{\rm e} = 5.54 \times 10^5$ K. The star's mass and radius are, resp., 1.4 $M_\odot$ and 10 km.

Two examples of such temperature distributions are illustrated in Figure 6. The overall effect on $T_{\rm e}$ is nevertheless surprisingly small, see, e.g., [66,67] and the examples in Figure 6, and a non-magnetic envelope is actually a rather good approximation. However, the assumption of spherical symmetry at $\rho > \rho_{\rm b}$ is questionable and will be discussed in § 7.

Given that the overall effect of the magnetic field, in the envelope, is not very strong, it turns out that the major uncertainty about the envelope is its chemical composition. The standard neutron star crust is made of cold catalyzed matter, which means ^{56}Fe at low density ($\rho < 10^6$ g cm^{-3}). However real neutron stars may be dirty and have lighter elements at their surface. As was shown in [68] the presence of light elements in the envelope strongly enhances heat transport (e.g., the electron thermal conductivity within liquid ions of charge Z, in the sensitivity layer, is roughly proportional to $1/Z$, [69]) and results in a significantly higher $T_{\rm e}$, for the same $T_{\rm b}$, than in the case of a heavy element envelope. Due to pycnonuclear fusion, light elements are unlikely to be present at densities above 10^9 g cm^{-3}. At very high $T_{\rm e}$ this density is below the sensitivity layer and light elements have little effect, but for $T_{\rm e}$ within the observed range ($\sim 10^5 - 10^6$ K) the sensitivity layer is at a sufficiently low density so that it can easily be contaminated with light elements and the $T_{\rm b} - T_{\rm e}$ relationship can be significantly altered. However, if only a small amount of light elements is present at the surface their effect will only be felt a low $T_{\rm e}$. We show in Figure 7 the $T_{\rm b} - T_{\rm e}$ relationships for various amounts of light elements and also, for comparison, the case of a magnetized

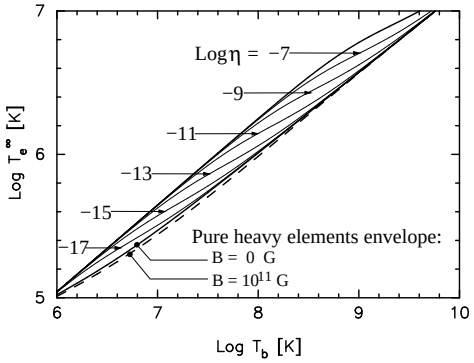

Fig. 7. Relationship between the red-shifted effective temperature $T_{\rm e}^{\infty}$ and the interior temperature $T_{\rm b}$ at the bottom of the envelope assuming various amounts of light elements parameterized by $\eta \equiv g_{\rm s\,14}^2 \Delta M_{\rm L}/M$ (M is the star's mass, $\Delta M_{\rm L}$ the mass in light elements in the envelope, and $g_{\rm s\,14}$ the surface gravity in units of 10^{14} cm s^{-2}; this figure assumes $g_{\rm s\,14} = 2.43$), in the absence of a magnetic field [70]. Also shown are the $T_{\rm b} - T_{\rm e}^{\infty}$ relationships for an envelope of heavy elements with and without the presence of a dipolar field of strength of 10^{11} G following [71]. Notice that the smaller is $\Delta M_{\rm L}$ the lower is the temperature at which its effect is felt.

envelope with a 10^{11} G dipolar magnetic field.

3 Some simple analytical solutions

Assuming simplified physics input one can easily obtain some very illustrative analytical solutions to the cooling Eq. (1). Let us write

$$C_{\rm v} = C \cdot T\,, \qquad L_{\nu}^{\rm slow} = N^{\rm s} \cdot T^8\,, \qquad L_{\nu}^{\rm fast} = N^{\rm f} \cdot T^6\,, \tag{9}$$

for the specific heat from degenerate fermions and neutrino emission with only "slow" processes or with some of the "fast" processes listed in Table 1. For L_{γ} we write

$$L_{\gamma} \equiv 4\pi R^2 \sigma_{\rm SB} T_{\rm e}^4 = S T^{2+4\alpha} \qquad \text{using} \qquad T_{\rm e} \propto T^{0.5+\alpha} \quad (\alpha \ll 1)\,, \tag{10}$$

where $T_{\rm e}$ has been converted into the internal temperature T through an envelope model with a power-law dependence. Figure 7 shows that for a heavy element envelope or for an envelope with a large amount of light elements this power-law relation is a good approximation in a wide range of temperatures. Typical values for the numerical coefficients in Eqs. (9) and (10) are listed in Table 3.

Due to the much stronger T dependence of L_{ν} compared to L_{γ}, at early times neutrino emission drives the cooling and when T has sufficiently decreased

Table 3
Typical numerical coefficients for simplified power-law cooling models

	C	$N^{\rm s}$	$N^{\rm f}$	S	α
	erg K^{-2}	erg s^{-1} K^{-8}	erg s^{-1} K^{-6}	erg s^{-1} K$^{-2-4\alpha}$	
high	10^{30}	10^{-32}	10^{-9}	4×10^{14}	0.1
low	10^{29}	10^{-34}	0	2×10^{15}	0.05

Comments:

C: "low" value corresponds to the leptons contribution only, i.e., assuming all baryons are paired with high $T_{\rm c}$'s, while "high" value corresponds to total absence of pairing.

$N^{\rm s}$: "high" value corresponds to total absence of pairing while "low" value assumes complete pairing of baryons in the core and neutrino emission is then provided predominantly by the electron-ion bremsstrahlung in the crust, which can also be very roughly approximated by a luminosity $\sim T^8$.

$N^{\rm f}$: "high" value corresponds approximately to an inner core of 1 $M_\odot$ sustaining a direct Urca process with nucleons, "low" value of course corresponds to total absence of fast neutrino emission.

S and α: "high" corresponds to an envelope with a maximum amount of light elements while "low" corresponds to an envelope made of heavy elements, in both cases with a stellar radius $R\sim12$ km.

photons will take over.

(1) During the **neutrino cooling era** we can neglect L_γ in Eq. (1) and, with our approximate formulas of Eq. (9), obtain analytical solutions

$$\left.\begin{array}{l}\text{Slow } \nu\\ \text{cooling}\end{array}\right\}:\quad t=\frac{C}{6N^{\rm s}}\left(\frac{1}{T^6}-\frac{1}{T_0^6}\right)\quad;\quad\left.\begin{array}{l}\text{Fast } \nu\\ \text{cooling}\end{array}\right\}:\quad t=\frac{C}{4N^{\rm f}}\left(\frac{1}{T^4}-\frac{1}{T_0^4}\right), \tag{11}$$

where T_0 is the initial temperature at time $t_0\equiv0$. For $T\ll T_0$, this gives, for slow ν cooling

$$T=\left(\frac{C}{6N^{\rm s}}\right)^{\frac{1}{6}}t^{-\frac{1}{6}}\qquad\text{and}\qquad T_{\rm e}\mathrel{\tilde{\propto}}t^{-\frac{1}{12}}, \tag{12}$$

and for fast ν cooling

$$T=\left(\frac{C}{4N^{\rm f}}\right)^{\frac{1}{4}}t^{-\frac{1}{4}}\qquad\text{and}\qquad T_{\rm e}\mathrel{\tilde{\propto}}t^{-\frac{1}{8}} \tag{13}$$

(we have used that $\alpha\sim0$). The very small exponent in the $T_{\rm e}$ evolution during neutrino cooling is a direct consequence of the strong temperature dependence of L_ν. The neutrino cooling time scales are also very suggestive:

$$\tau_\nu^{\rm slow}=\frac{C}{6N^{\rm s}T^6}\simeq6\text{ months}\cdot\left[\frac{C_{30}}{6N^{\rm s}_{-32}T_9^6}\right], \tag{14}$$

and

$$\tau_\nu^{\rm fast} = \frac{C}{4N^{\rm f}T^4} \simeq 4 \text{ minutes} \cdot \left[\frac{C_{30}}{6N^{\rm f}_{-9}T_9^4}\right] , \tag{15}$$

and justify the names of "slow" and "fast" neutrino cooling! Notice that 10^9 K is a typical value for the baryon pairing $T_{\rm c}$, and hence, in case of fast neutrino cooling, one can expect that a few minutes after the star is born its core may become superfluid/superconducting, and the neutrino emission very strongly suppressed.

(2) During the **photon cooling era** ($L_\gamma \gg L_\nu$) one similarly obtains

$$t = t_1 + \frac{C}{4\alpha\, S}\left(\frac{1}{T^{4\alpha}} - \frac{1}{T_1^{4\alpha}}\right) , \tag{16}$$

where T_1 is the temperature at time t_1. When $t \gg t_1$ and $T \ll T_1$, we have

$$T = \left(\frac{C}{4\alpha S}\right)^{\frac{1}{4\alpha}} t^{-\frac{1}{4\alpha}} \quad \text{and} \quad T_{\rm e} \mathrel{\widetilde{\propto}} t^{-\frac{1}{8\alpha}} . \tag{17}$$

Since $\alpha \ll 1$, we see that, during the photon cooling era, the evolution is very sensitive to the nature of the envelope, i.e., α and S, and to changes in the specific heat, as induced by pairing. Notice that in case $\alpha = 0$ one would obtain an exponential solution instead of a power law.

The **shift from neutrino to photon cooling:** the temperature $T_{\rm shift}$ at which this happens is also easily estimated by equating L_ν to L_γ, giving for slow ν cooling

$$T^{\rm s}_{\rm shift} \simeq \left(\frac{S}{N^{\rm s}}\right)^{1/6} \sim 10^8 \text{ K} \quad \text{and} \quad T_e \sim 10^6 \text{ K} \tag{18}$$

and for fast ν cooling

$$T^{\rm f}_{\rm shift} \simeq \left(\frac{S}{N^{\rm f}}\right)^{1/4} \sim 10^6 \text{ K} \quad \text{and} \quad T_e \sim 10^5 \text{ K} \tag{19}$$

However, for fast ν cooling $N^{\rm f}$ can be significantly reduced by pairing and hence $T^{\rm f}_{\rm shift}$ increased. One may also want to obtain an estimate of the age $t_{\rm shift}$ at which this happens by using Eq. (12) and (13). It is however now important to keep the α dependence in L_γ, Eq. (10), and, for small α one obtains, for slow ν cooling, $t^{\rm s}_{\rm shift} = C/6S(N^{\rm s}/S)^{(2/3\,\alpha)}$ and a similar expression

for fast ν cooling. Given that N/S is a *very* small number, the value of $t_{\rm shift}$ is extremely sensitive to the exact value of α, and also of N which can be altered by several orders of magnitude by pairing. Considering moreover that these simple solutions are based on approximate formulas, such results for $t_{\rm shift}$ are not very useful in themselves for numerical estimates but show that $t_{\rm shift}$ can change significantly by small changes in the interior (through N and C) and/or surface (through S and α) physics. The numerical results presented in the following sections show that $t_{\rm shift}$ can vary from about 10^4 yrs up to about 10^6 years, for both slow and fast ν cooling.

4 The "Minimal Cooling" paradigm

The Minimal Cooling paradigm assumes that no enhanced neutrino emission is allowed, in particular, that no form of "exotic" matter is present in the inner core of the star. It is hence a benchmark against which observations of cooling neutron stars have to be compared, and a discrepancy between the minimal cooling theoretical predictions and data should be considered as strong evidence for physics beyond minimal. As such the minimal paradigm excludes *a priori* the presence of charged meson condensates, hyperons, and/or deconfined quark matter, but it also assumes that the growth of the symmetry energy with density is slow enough that the nucleon direct Urca process is forbidden. It can be seen as a modern version of the "Standard Cooling" scenario but with the important difference that the effects of nucleon pairing are wholly taken into account, particularly the strong neutrino emission from the formation of Cooper pairs during the pairing phase transition [4] .

This paradigm is studied in great detail in Ref. [2]. Its tenets immediately imply strong constraints on the supernuclear equation of state, resulting in stellar radii between 11 to 12 km for a 1.4 $M_\odot$ mass and between 9 to 10 km at the maximum mass (the latter being not so strongly constrained, around 1.7 up to 2.3 $M_\odot$). Neutrino emission from the core comprises the neutron and proton branches of the modified Urca processes and the similar, but less efficient, *n*-*n*, *n*-*p*, and *p*-*p* bremsstrahlung processes (see Table 1), which are inherited from the old "standard" scenario. However, essential and unavoidable within the minimal scenario is the occurrence of nucleon pairing. The resulting suppression of both the nucleonic specific heat and the above mentioned neutrino emission processes is well known, but a result is that neutrino emission by the PBF process is dominating for most cases of pairing gaps. This is illustrated in Figure 8: the left panel clearly shows that for $T_{\rm c}$'s of the

[4] The motivation for the renaming from "Standard" to "Minimal" is precisely that "Standard Cooling" is commonly understood as "Modified Urca Cooling" while, in presence of pairing, the dominant process is the PBF process.

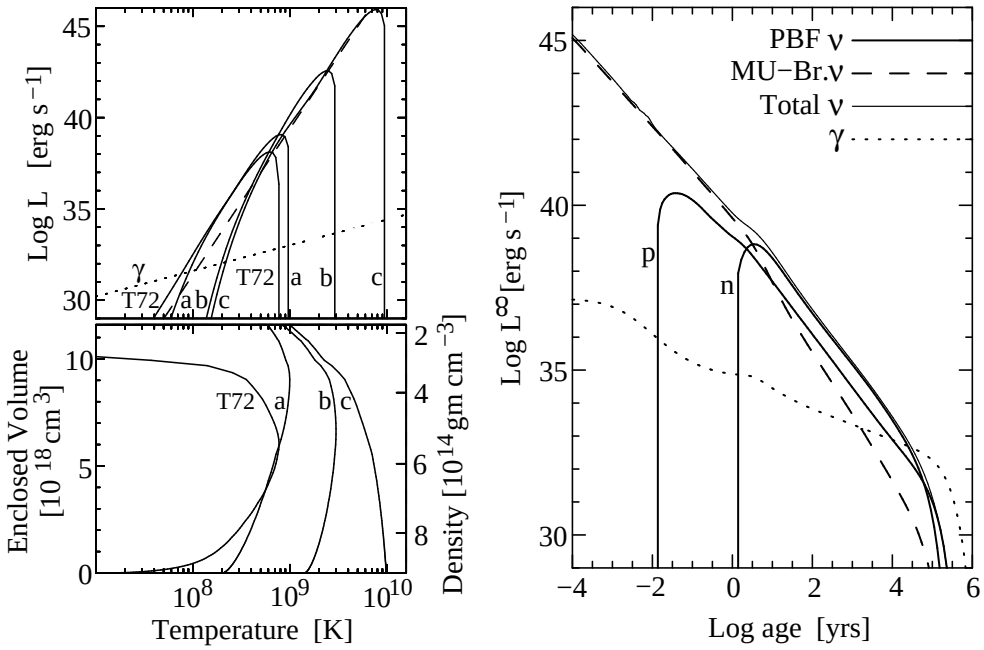

Fig. 8. Left Panel: neutrino luminosities from the PBF process for four different neutron ${}^3P_2 - {}^3F_2$ gaps (labeled "a", "b", and "c' as in Figure 4 while the gap labeled "T72" is taken from [72]). The lower left panel shows the four gaps' $T_{\rm c}$ vs. the enclosed volume (left scale) and density (right scale) and the upper left panel the corresponding PBF luminosities as well as the surface photon luminosity while the dashed curve shows, for comparison, the total luminosity from modified Urca and nucleon bremsstrahlung processes *without pairing suppression*. Luminosities are calculated assuming an isothermal star so that, e.g., with a temperature of 2×10^9 K, one can see that in case of gap "b", two regions have unpaired neutrons: the inner core at ρ above $\sim 8.5 \times 10^{14}$ g cm^{-3} and a corresponding volume of $\sim 1.1 \times 10^{18}$ cm^3, and the outer core at ρ below $\sim 3 \times 10^{14}$ g cm^{-3} and corresponding volume of about $\sim (11.5 - 9.8) \times 10^{18} \simeq 1.7 \times 10^{18}$ cm^3, while the intermediate region, of volume $\simeq 9 \times 10^{18}$ cm^3 has T slightly below T_c and produces the large L_ν by the PBF process shown in the upper panel. Right panel: comparison of luminosities from various processes during a realistic cooling history: photon ("γ"), all ν-processes ("Total ν"), modified Urca and nucleon bremsstrahlung ("MU-Br. ν"), and PBF ("PBF ν") from $n\ {}^3P_2 - {}^3F_2$ and $p\ {}^1S_0$ pairing marked by "n" and "p", respectively. The $n\ {}^3P_2 - {}^3F_2$ gap is our model "a" which, as shown on the left panel, is amongst the most efficient one for the PBF process while the $p\ {}^1S_0$ gap is from [73]. All results are from Ref. [2].

order of 10^9 K, as in the cases "a" and "T72", the PBF process is more than one order of magnitude more efficient than the *unsuppressed* modified Urca and bremsstrahlung processes when T is below T_c. Once the pairing suppression of these last two processes are taken into account the PBF process can dominate by up to two orders of magnitude as shown in the right panel of Figure 8. The left panel of Figure 9 compares the effects of various neutron ${}^3P_2 - {}^3F_2$ gaps, confirming the results of the previous figure that $T_{\rm c} \sim 10^9$ K

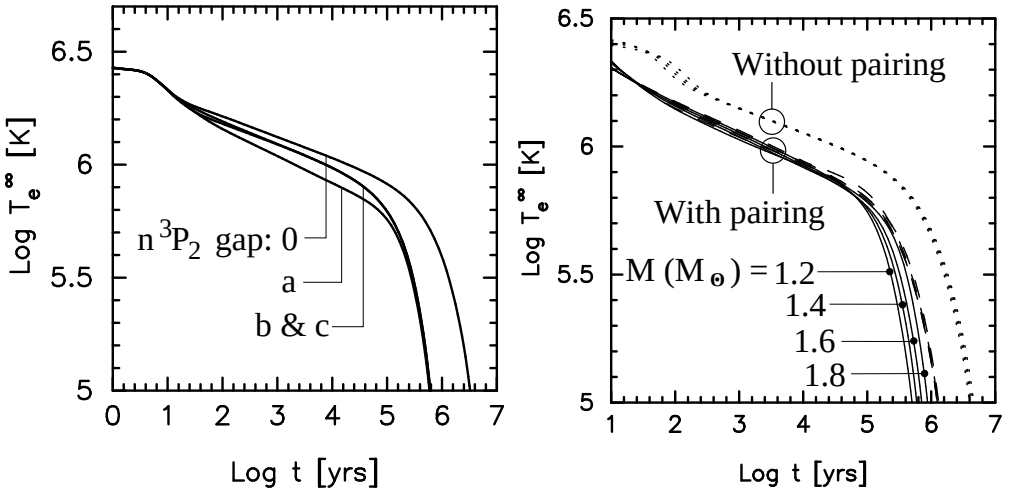

Fig. 9. Minimal cooling. Left panel: comparison of cooling trajectories with vanishing $n\ ^3P_2 - {}^3F_2$ gaps, labeled "0", and the three model gaps "a", "b", and "c" (see Figure 4). Right panel: dependence of the cooling trajectory on the stellar mass without pairing, where the mass effect is almost indistinguishable, and with only proton $^1S_0$ pairing (dashed curves) and both proton $^1S_0$ and neutron $^3P_2 - {}^3F_2$ pairing. Results from Ref. [2].

provides the strongest PBF neutrino cooling, while the right panel consider the effect of the stellar mass, which turns out to be rather weak. Only in case of extensive nucleon pairing can we find some small mass dependence.

Comparison of the predictions of the Minimal Cooling paradigm with the data is shown in Figure 10. Predictions assuming a heavy element or a light element envelope are plotted separately and, for each envelope model, the width in the predictions is a result of the uncertainty in the size of the nucleon pairing gaps. Each wide grey strip encompasses the whole range of results when all gaps shown in Figure 4 are used. The small mass dependence is also included in these results. Objects with the best data, shown as boxes in the figure, show a remarkably good agreement with the theoretical results of the minimal cooling. One may still focus on two stars, PSR 1055–52 and RX J0720.4–3125, which may be warmer than predicted and could be cases in which some internal heating mechanism is at work. On the other side, PSR 0833–45 ("Vela") and PSR 1706–44, may be too cold and require some enhanced neutrino emission. However, much stronger cases for the necessity of enhanced neutrino emission are the two pulsars PSR J0205+6449 and RX J0007.0+7302 which are clearly below any of the predictions of the minimal cooling paradigm. Finally, the upper limits on the luminosity of the neutron star which may be present in the four SNRs marked as "a", "b", "c", and "d" in this figure doubtlessly require enhanced neutrino emission in case any of these SNRs contained a neutron star. Similar results has been recently obtained in Ref. [74] which, with *ad-hoc* gaps, showed that even PSR J0205+6449 and RX J0007.0+7302 could be accommodated within the minimal paradigm.

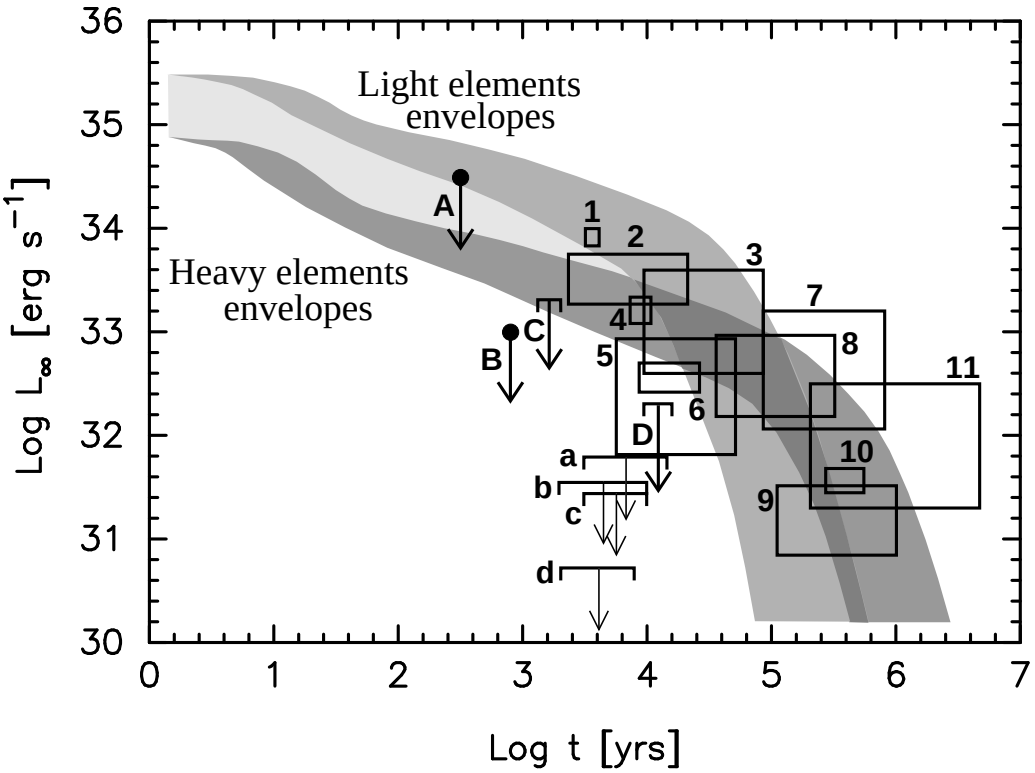

Fig. 10. Comparison of the predictions of the Minimal Model of neutron star cooling with the best presently available data. The two dark grey shaded areas correspond to models having a heavy element envelope or an envelope with a maximum amount of light elements, as labeled, and the light grey area indicate intermediate trajectories corresponding to intermediate amounts of light elements in the envelope. The spread of predictions, for each envelope type, corresponds to different assumptions about the extent of nucleon (neutron and proton) pairing. Boxes correspond to neutron stars where surface thermal emission is clearly detected and which have been studied in detail: 1 to 6 are obtained from spectral fits with magnetized hydrogen atmospheres while 7 to 11 are from blackbody fits. These stars are: 1 - RX J0822–4247 (in SNR Puppis A), 2 - 1E 1207.4–5209 (in SNR PKS 1209–52), 3 - PSR 0538+2817, 4 - RX J0002+6246 (in SNR CTB 1), 5 - PSR 1706–44, 6 - PSR 0833–45 (in SNR "Vela"), 7 - PSR 1055–52, 8 - PSR 0656+14, 9 - PSR 0633+1748 ("Geminga"), 10 - RX J1856.5–3754, and 11 - RX J0720.4–3125. The next four stars, labeled as A, B, C, and D, are barely detected and in case C there is no evidence for thermal emission: A - CXO J232327.8+584842 (in SNR Cas A), B - PSR J0205+6449 (in SNR 3C58), C - PSR J1124–5916 (in SNR G292.0+1.8), and, D - RX J0007.0+7302 (in SNR CTA 1). The last four data points, a, b, c, and d, are from deep observations of four shell SNRs, considered as products of core collapse supernovae, in which there is no evidence of any kind for the presence of a compact object; they may correspond to very cold neutron stars or isolated black holes: a - ? (in SNR G315.4–2.3), b - ? (in SNR G093.3+6.9), c - ? (in SNR G084.2–0.8), and, d - ? (in SNR G127.1+0.5). See Ref. [2] for discussion and references.

5 Enhanced Cooling

In the core, almost any chemical composition beyond the one of the minimal scenario will open channels for enhanced neutrino emission which possibly results in extremely fast cooling of the neutron star. The left panel of Figure 11 illustrates the effect of the direct Urca process from nucleons in a model where this process is allowed for masses above 1.35 $M_\odot$ (this specific critical mass is of course very model dependent). Notice that the 1.4 $M_\odot$ star has an inner "pit" where the direct Urca process is occurring with a mass of only 0.038 $M_\odot$, while the 1.7 $M_\odot$ star's "pit" is above 1 $M_\odot$. After the early phase, at ages a few tens of years, the rapid temperature drop in fast cooling stars is due to the finite thermal relaxation time of the crust and heavier stars, having thinner crusts, relax faster. The right panel of this figure compares the impact of the direct Urca process on stellar cooling with other enhanced cooling processes, which originate from pion condensation, kaon condensation and the direct quark Urca process. Differences between these models come as much from the various efficiencies for neutrino emission as from the various critical densities at which enhanced emission becomes allowed. Comparison with the data plotted here shows that any of these fast cooling processes results in stars with temperature clearly incompatible with observations.

This naive picture is strongly affected when baryon pairing is taken into account [31,75,76]. As discussed in § 2.3 the development of an energy gap induces a suppression of the neutrino emission for any process in which the paired component participates. As can be seen from the left panel in Figure 12, neutron superfluidity ($^3P_2 - {}^3F_2$ in the present example with a small superfluid gap of 0.3 MeV [5]) delays cooling significantly and moves the theoretical temperatures right up to the region where most observed data are concentrated. Similar results are obtained with all enhanced cooling scenarios as, e.g., nucleon direct Urca [76], K^- or π^- condensates [31,77,78], hyperons [79–81] or hyperons with deconfined quarks [81]. With a high enough value of $T_{\rm c}$ the enhanced neutrino emission may not even have time to act and result in stellar temperatures as high as the ones obtained within the minimal scenario [76].

The right panel of Figure 12 illustrates several of these considerations [81]. This panel shows cooling curves for models with only nucleons (thin continuous curves) and with nucleons and an hybrid phase of nuclear+deconfined quark matter (dashed curves and dotted curves) and various hypotheses about pairing. Nucleon and quark direct Urca processes are allowed, except in the case marked as "Mc" where they are arbitrarily turned off for illustration. Four different neutron $^3P_2 - {}^3F_2$ gaps are considered, labeled as "z" (zero gap), and "a", "b", and "c" according to Figure 4. For models including quark matter in the inner core, five quark gaps are also considered, labeled as "Z" (zero gap),

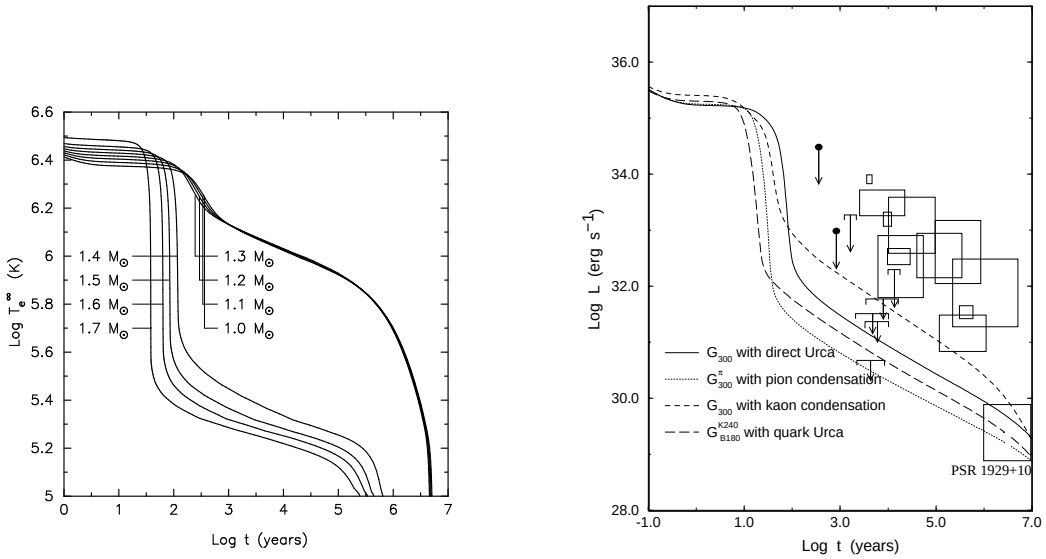

Fig. 11. Left panel: influence of the direct Urca process on the cooling of stars of various masses. (Figure from Ref. [76].) Right panel: influence of different enhanced neutrino emission processes on the cooling of neutron stars of mass $M = 1.4\,M_\odot$, except for the kaon-condensed model whose mass is $M = 1.8\,M_\odot$. (The $1.4\,M_\odot$ model is not dense enough to support a kaon condensation). (Figure from Ref. [33].) Upper limit on PSR 1929+10 thermal luminosity is from Ref. [83]; see Figure 10 for identification of other data.

"A", "B","C", and "D" corresponding, to maximum gap sizes of 0.1, 1.0, 10, and 100 MeV, respectively (all flavors and color of quarks are assumed to have the same gap for simplicity). Considering models without quarks matter (continuous lines), one sees that models with a large neutron ${}^3P_2 - {}^3F_2$ gap "c" have almost the same evolution as the model with no direct Urca process, "Mc", and are all compatible with the highest measured neutron stars temperatures. Models with neutron gap "b" could explain, as in the left panel, the intermediate temperature neutron stars, in which case the warmer one should be understood as having lower masses and no direct Urca process allowed (model "Mc"). Models with smaller neutron gaps produce too low temperatures but would correspond to the four upper limits (data points labeled as "a", "b", "c", and "d" in Fig 10). Finally, hybrid models with quarks (dashed and dotted lines) give almost indistinguishable results when the quark gaps are large enough (curves labeled "A", "B", "C", and "D") and it is only in case of a vanishingly small quark gap that their presence is noticeable.

As can be seen from this brief presentation, we have an embarrassingly large number of possible scenarios in case enhanced neutrino cooling is occurring. Most models have to include in an essential way the various possible pairing gaps, about which very little is known at high densities, to reconcile enhanced neutrino cooling with data. Nevertheless there are possibilities to have a smooth transition from slow to fast neutrino cooling through strong medium effects and without invoking pairing [23,82], or with a significant amount of

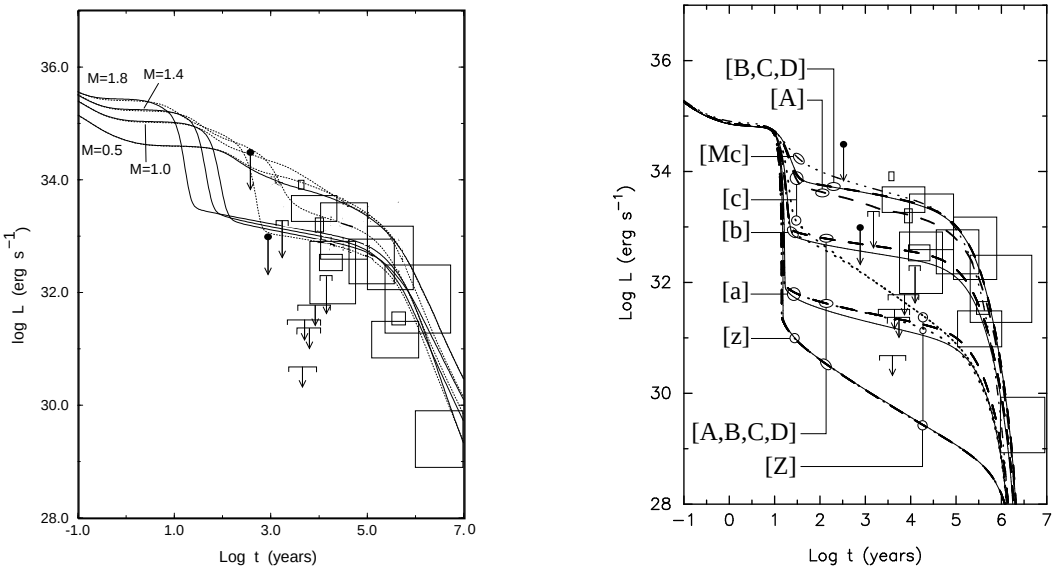

Fig. 12. Left panel: influence of superfluid $^3P_2 - {}^3F_2$ neutrons on the cooling curves labeled G^{π}_{300} and G_{300} (with kaon condensation) in Figure 11 for various neutron star masses. (Figure from Ref. [33].) Right panel: effect of varying the neutron and quark gap size, while keeping the mass fixed at 1.4 $M_{\odot}$. See text for description and discussion. (Figure from Ref. [81].) The large differences in luminosities at late times between the two panels are due to small differences in treatment of the envelope and specific heat, as discussed after Eq. (17). See Figures 10 and 11 for identification of data.

internal heating as discussed in § 8. Obviously, much work is still needed to determine which scenarios are the more plausible.

6 Cooling of Strange Quark Stars

6.1 Strange Stars with Nuclear Crusts

If strange quark matter were in fact the true ground state of the strong interaction (see § 2.1), new classes of compact stars should exist which range from dense strange stars to strange dwarf stars [84,85]. They would form distinct and disconnected branches of compact stars and are not part of the continuum of equilibrium configurations that include ordinary white dwarfs and neutron stars [86]. Figure 13 shows the cooling behavior of such strange stars with and without nuclear crusts. One sees that not even the thickest, theoretically possible crust (inner crust density equal to neutron drip density) does prevent strange stars from cooling very rapidly [87]. If one treats the quarks as superfluid particles, assuming a small density-independent gap of just 0.1 MeV, radiation of neutrinos is greatly reduced and the stellar cooling behavior is

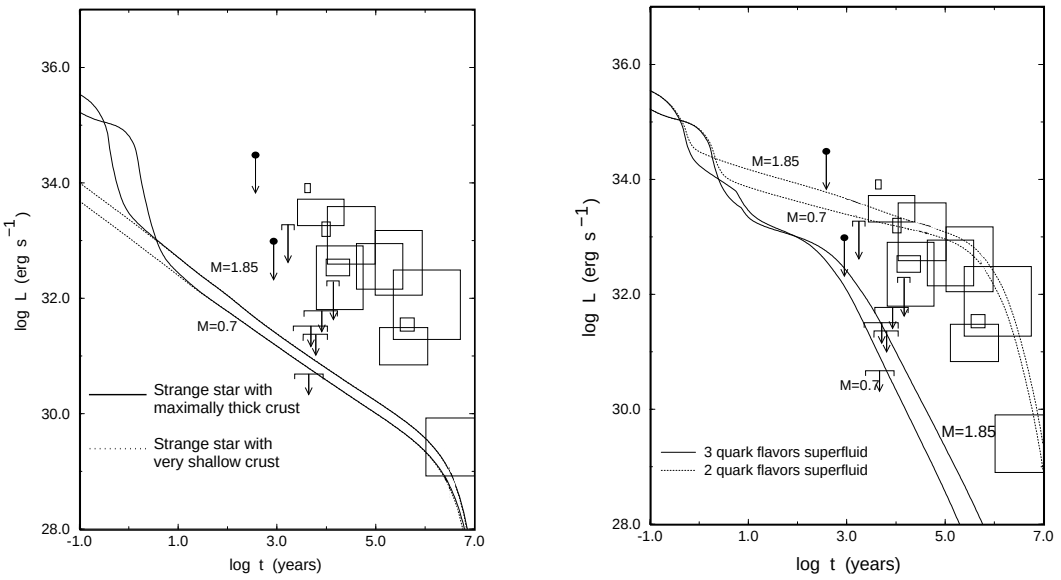

Fig. 13. Cooling behavior of strange stars with maximally thick crusts and with very thin crusts, i.e., with only an envelope (Figure from Ref. [33].) See Figure 10 and 11 for identification of data.

rather similar to that of conventional neutron stars. The different condensation patterns of color superconducting quark matter, discussed in § 2.4, do not alter this picture dramatically. In the CFL phase, for instance, all quarks have very large gaps, $\Delta \gg T$, so that both ϵ_ν and $c_{\rm v}$ are so strongly reduced that quark matter that may exist in the center of a neutron star would be rendered invisible. Notice that, in spite of the CFL phase being charge neutral by itself in bulk [88], a strange star in the CFL can still support a nuclear crust when surface boundary conditions are properly taken into account [89]. The cooling behavior of such stars would then be determined by the nuclear matter surrounding the CFL quark matter core. This conclusion is strengthened by the studies performed in Refs. [90,91]. The cooling behavior of compact stars with 2SC quark matter in their cores is simplified by the fact that up and down quarks may pair with a gap $\Delta \sim 100$ MeV which is orders of magnitude larger than the stellar temperature, $\lesssim 1$ MeV, and are therefore inert with respect to the star's temperature evolution. For 2SC quark matter, however, there exist also quark pairing channels that lead to weak pairing with gaps on the order of several keV to about 1 MeV, which is on the same order of magnitude as the star's temperature. These quarks may thus not pair but, instead, radiate neutrinos rapidly via the quark direct Urca process (Table 2). If this is the case, the 2SC quark matter core would cool rapidly and determine the cooling history of the star [56,92]. Naturally the cooling behavior of such stars depends rather sensitively on the value of the superfluid gap [92].

6.2 Strange Stars with a Bare Quark Surface

Even though it is in principle possible to cover the strange quark matter by a layer of normal nuclear matter, as assumed in the previous subsection, it is not clear at all how such a nuclear crust may be formed. When a strange star is born its internal temperature is likely of the order of a few times 10^{11} K, as in a standard proto-neutron star formed in core-collapse, and the resulting neutrino flux is so high that it should easily be able to expel all baryonic matter surrounding the quark matter [93]. As a result a new-born strange star is most certainly *bare*, i.e., its surface consists directly of quark matter with no nuclear component above it. Such a strange star remains bare as long as its temperature is above $\sim 3 \times 10^7$ K [94].

If this is the case, the thermal evolution of a bare strange star would be radically different from the one of a neutron star or a strange star with a crust. The surface density of the quark matter is about $4 - 8 \times 10^{14}$ g cm^{-3} and the resulting plasma frequency of the order of 20 MeV [19] which may lead one to believe that a bare strange star is unable to emit thermal radiation once it's temperature dropped below about 10^{10} K, i.e., a few seconds after its birth: a bare strange star would be a silver sphere instead of a blackbody emitter. However this naive picture neglects the presence of electrons within the quark matter which are bound to the quark matter by Coulomb forces. As such, the electrons slightly leak out of the quark matter, by a distance which is roughly given by their Debye screening length, producing thus an electrosphere with a thickness of a few thousand Fermis [95]. As noted by Usov [96] the resulting electrostatic field, of the order of 5×10^{17} V cm^{-1} [19], is well above the Schwinger critical field of QED and can induce copious production of $e^- - e^+$ pairs at the surface. However, this pair emission does not occur in vacuum, but within the electrosphere and it is ultimately limited by electron degeneracy. Nevertheless the resulting luminosity is enormous as long as the surface temperature is above $\sim 10^9$ K [97]. Pairs outflowing from the stellar surface mostly annihilate into photons in the vicinity of the strange star [97] resulting in a fireball of e^-, e^+ and γ's. At luminosities $> 10^{41}$ erg s^{-1} this plasma is optically thick and produces a blackbody spectrum while at decreasing luminosities the spectrum progressively evolves into a very wide annihilation line [98]. At lower temperatures, when pair production becomes suppressed by electron degeneracy, photons can still be emitted by $e^- - e^+$ bremsstrahlung within the electrosphere [99] and result in significant luminosities.

The thermal evolution of a bare strange star with the Usov-Schwinger pair production mechanism has been studied numerically in [100] and results are shown in Figure 14. Uncertainties about the pairing state of quark matter are taken into account schematically in the three scenarios marked in the figure as "A", "B", and "C", in which the gaps suppress neutrino emission with

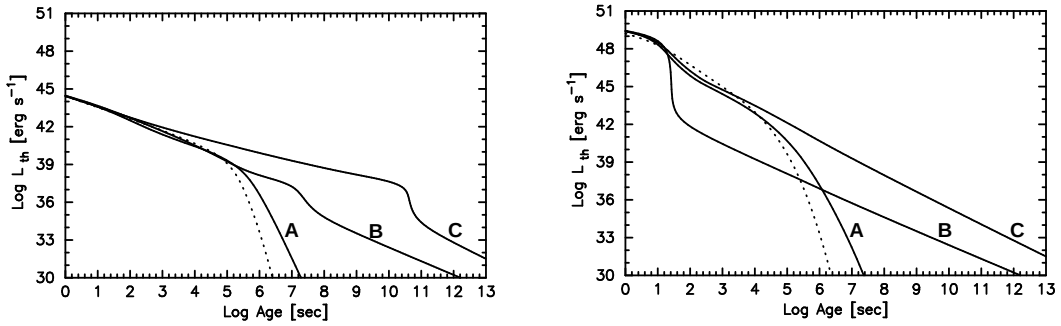

Fig. 14. Cooling behavior of a bare strange star, showing the thermal luminosity from the Usov-Schwinger pair-production mechanism vs. age. In the left panel it is assumed that heat, within the star, flows to the surface by diffusion while in the right panel convection is allowed resulting in much stronger heat flow and higher thermal luminosities. In the dotted curves no quark superconductivity is included while the continuous curves labeled A, B, & C have quark color superconductivity taken into account for three possible scenarios (see text for details). (From Ref. [100].)

increasing efficiency, leading thus to slower cooling of the star. These results show that bare strange stars can produce extremely high thermal luminosities, well above the Eddington limit, over extended periods of time, but with considerable uncertainty due to the precise phase of color superconductivity present at these "low" astrophysical densities. Notice, however, that the photon emission from $e^- - e^+$ bremsstrahlung in the electrosphere [99] was not included in these models, and will significantly change the evolution when the thermal luminosity has dropped below 10^{40} erg s^{-1}.

7 Magnetic field effects in the crust

All the heat stored in the core of the neutron star and eventually irradiated away from its surface by photons has to be transported through the crust. In the absence of rotation and magnetic field this transport in the crust is spherically symmetric. While the effects of rotation are quite small even for millisecond pulsars, the presence of magnetic fields may cause significant deviations from the spherical symmetry of the transport processes, even for quite "standard" field strength of $\sim 10^{12}$G. Due to the classical Larmor rotation of electrons, a magnetic field causes anisotropy of the heat flux and the heat conductivity becomes a tensor whose components perpendicular, $\kappa_\perp$, and parallel, $\kappa_\parallel$, to the field lines are given by

$$\kappa_\perp = \frac{\kappa_0}{1 + (\Omega_B \tau)^2} \quad \text{and} \quad \kappa_\parallel = \kappa_0 \ , \tag{20}$$

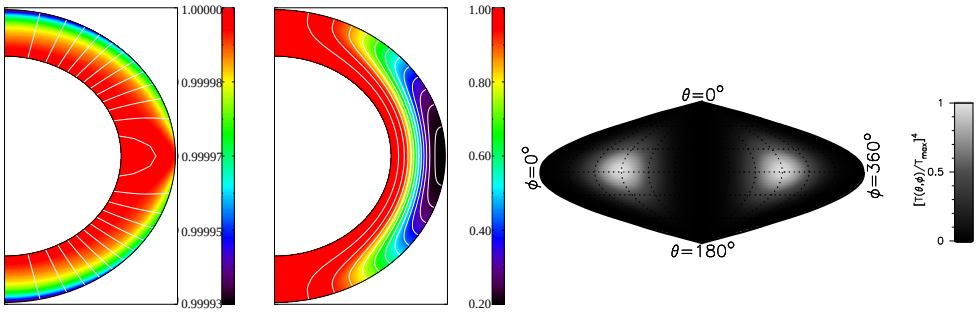

Fig. 15. Temperature distribution and magnetic field lines in the crust for a "core" (left panel) and a "crustal" (central panel) dipolar field (from Ref.[101]), and surface temperature distribution resulting from the "crustal" field (right panel). The "core" field gives a surface temperature distribution very similar to the left panel of Figure 6. The thickness of the crust in left and central panels has been stretched by a factor 5 for clarity and the two bars show the temperature scales in units of $T_{\rm core} = 10^6$ K. For the "core" field on has $T_e = 1.15 \times 10^5$K while for the "crustal" field $T_e = 0.89 \times 10^5$K. In both cases, the dipolar field strength is $B_0 = 3 \times 10^{12}$ G at the magnetic pole. (The neutron star considered here has a 1.4 $M_\odot$ mass and a radius of 11 km.)

where κ_0 is the conductivity in absence of magnetic field, Ω_B the gyro-frequency of the electrons and τ their collisional relaxation time. In the neutron star crust $\Omega_B \tau \gg 1$ is easily realized and, as a result, heat flows preferentially along the magnetic field lines [101]. This effect is moreover amplified at the surface by the well known non-isotropy in the envelope as described in § 2.6.

The non-isothermality of the subjacent crust depends strongly on the internal geometry of the field [101]. Assuming a dipolar field structure, outside the star the radial dependence of the field is uniquely determined, $\propto r^{-3}$, while inside the star it depends on the location of the electric currents, through Ampère's law. Assuming currents are exclusively located in the core ("core field") the r^{-3} dependence also applies to the crust while if they are exclusively located in the crust and the field does not penetrates the core ("crustal field") the field topology in the crust is radically distinct: for the *same* external field in the latter case field lines in the crust are squeezed into the crustal shell and have hence a very large meridional component. This meridional component of the crustal field inhibits the radial flow of heat which is hence redirected preferentially toward the magnetic poles. This difference is illustrated in Figure 15.

The drastic difference in the crustal temperature distribution for the different field structures which are characterized by the same dipolar field structure and strength outside the neutron star, causes significant differences in the surface temperature distribution which will have several observational consequences:

1. A non-uniform surface temperature induces a modulation of the observed soft X-ray thermal emission [66]. The stronger channeling of the heat flow toward the polar regions in the case of a crustal field will result in larger amplitude in the pulse profile.

2. The differences in the photon luminosities for a core or a crustal field will also affect the long term cooling of neutron stars. A neutron star having a magnetic field confined to its crust will stay warmer for a longer time, due to its lower photon luminosity, compared to a neutron star with a field penetrating its core.

3. This may open a way to study the *internal* geometry of the magnetic field. We may be able to distinguish between field geometries where the currents are essentially localized in the crust or in the core, or even detect the imprint of the presence of a toroidal field [102].

8 Heating Mechanisms

The expression "heating mechanism" refers to the term "H" in Eq. (1) and generically encompasses all possible dissipative processes which will inject heat into the star by tapping into various forms of energy: magnetic (§ 8.1), rotational or chemical (§8.2).

8.1 Magnetic Field Decay and Joule Heating

Given that most neutron stars have strong magnetic fields, magnetic energy is a natural reservoir from which to extract heat by the Joule effect from the decaying electric currents. Assuming a uniform internal field of strength $B = 10^{13} B_{13}$ G, one can roughly estimate an amount

$$E_{\rm mag} \sim \frac{B^2}{8\pi} \times \frac{4}{3}\pi R^3 \sim 2 \times 10^{43}\ B_{13}^2\ \ {\rm erg} \tag{21}$$

of stored magnetic energy. With a field decay time scale $\tau = 10^6 \tau_6$ yrs this gives us an equivalent "magnetic heating luminosity"

$$H_{\rm mag} \simeq \frac{E_{\rm mag}}{\tau} \sim 6 \times 10^{29}\ \frac{B_{13}^2}{\tau_6}\ \ {\rm erg\ s^{-1}} \tag{22}$$

This simple estimate indicates that decay of a standard magnetic field can alter the neutron star thermal evolution at late ($> 10^6$ yr) times. In the case

of a magnetar, ultra-strong fields and potential channels for fast decay (i.e., $\tau \ll 10^6$ yrs) can nevertheless lead to significant heating in young stars [103–105].

We will now describe some numerical results for the simplest case of a standard magnetic field, following the Ref. [106] which considered the case where magnetic energy is converted into heat through Ohmic decay of the currents supporting the field. This Joule heating contributes to the source term H in Eq. (1), where the heat production by field decay per unit of (proper) time and volume is given by $\vec{j}^2/\sigma$, $\vec{j}$ being the electric current density and σ the scalar electric conductivity. Joule heating is specially effective in the crust, which never becomes superconductive. Therefore, Ref. [106] considered only magnetic fields which are, along with the currents supporting them, confined to the neutron star crust and some results are shown in Figure 16 (see also Ref. [107]). The amount of heat locally released by Joule heating is determined by the strength of the field and its decay rate at that time. Most of the magnetic energy is dissipated at early times when it has almost no effect because the star's thermal energy is still too large. It is only when the star has become sufficiently cold that $H_{\rm mag}$ becomes significant, unless the field strength is of magnetar size. As illustrated in Figure 16, scenarios with a weak field supported by currents located at low density, i.e., decaying fast while the star is still hot, lead to virtually no observable effect. On the contrary, scenarios with strong field supported by currents at high densities keep a large amount of magnetic energy to be dissipated on long time scales, the best cases being fast cooling stars which result in the highest temperatures at ages $\sim 10^7 - 10^8$ years.

The above description is based on a linear evolution of the field but non-linear effects caused by the Hall drift in the highly magnetized crust may lead to an instability, which transfers magnetic energy rapidly from large scale structures into much smaller ones [108,109]. In that way, close to the NS surface small scale ($\sim 0.1 - 1$ km) field structures, as necessary for the onset of the pulsar mechanism, will be created which simultaneously are sources of accelerated ($t_{\rm Hall} \sim 10^4$yrs) Joule heating [110]. Detailed numerical modeling of the effect of this instability on the cooling of the pulsar remains to be performed.

8.2 Dissipative motion of vortex lattices and readjustment to equilibrium

The dissipative motion of vortex lattices and the rotational readjustment of the stellar equilibrium structure are other key processes that contribute to the heating of neutron stars. The relative effectiveness of these heating processes, however, varies significantly from one process to another, and depends sensitively on the value of the rotational parameter K, which enters the power-law

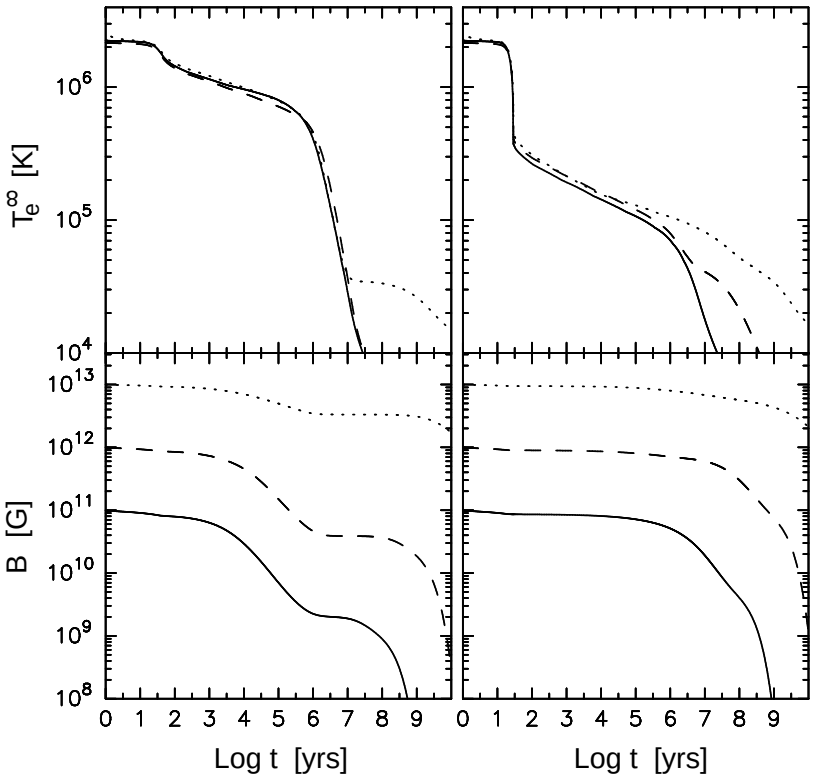

Fig. 16. Thermal (upper panels) and magnetic (lower panels) evolutions of neutron star undergoing slow (left panels) and fast (right panels) neutrino cooling, with Joule heating from magnetic field confined to the stellar crust. The three representative cases of initial field strengths cover a wide range of model parameters: $B_0 = 10^{11}$, 10^{12}, and 10^{13} G have their supporting currents initially concentrated at densities of $\rho_0 \sim 10^{12}$, 10^{13}, and 10^{14} gm cm^{-3}, respectively. (Adapted from Ref. [106].)

relation $\dot{\Omega}(t) = -K(t)\Omega^n(t)$ characterizing the spin-down of pulsars. Figure 17 shows the heating rate H (which enters in Eq. (1)) computed for several competing internal heating processes and parameter sets. These are [111]: vortex creep dissipation with pinning at nuclei for A) the Epstein-Baym parameter set (EB-pinning) and B) the parameter set of Pizzochero et al.; vortex flow dissipation C) in the crust and D) in the core; E) crust cracking; and F) chemical heating. Notice that the parameters values in case A) probably overestimate the effect. Chemical heating occurs because of the changing chemical composition with stellar frequency. The matter would maintain chemical equilibrium if the relaxation timescales for the weak reaction processes were small compared to the timescale of rotational evolution. These timescales, however, were found to be comparable and the stellar composition therefore departs from chemical equilibrium, which modifies the reaction rates [112] and leads generally to a net conversion of chemical energy into thermal energy [113,114]. In general, internal heating leads to enhanced stellar surface temperatures, which can be very pronounced for rotating neutron stars of middle ($K \sim 10^{-15}$ s) and old ($K \sim 10^{-22}$ s) ages [111] or millisecond pulsars [115]. As shown in [111,116]

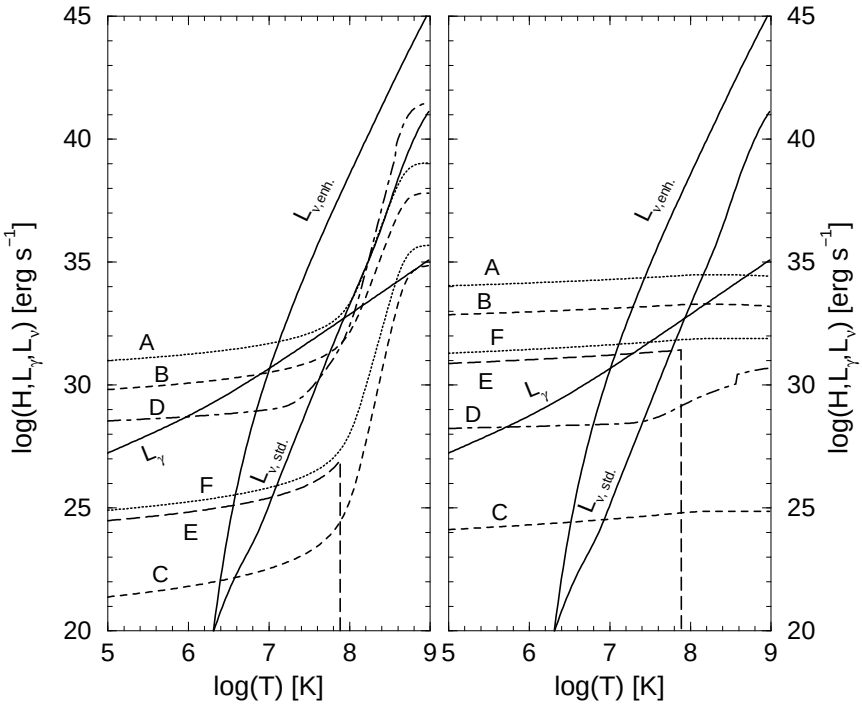

Fig. 17. Heating rate H as a function of internal star temperature for the heating scenarios (A)–(F) listed in the text. The left panel corresponds to $K \sim 10^{-15}$ s, the right panel to $K \sim 10^{-22}$ s. The photon and neutrino luminosities of standard cooling and enhanced cooling models (L_γ, $L_{\nu,\,\mathrm{std.}}$, $L_{\nu,\,\mathrm{enh.}}$) are shown for comparison. (Figure from Ref. [111].)

(see also [117]), the increase in surface temperature caused by the internal heating due to thermal creep of pinned vortices and the outward motion of proton vortices in neutron stars cooling rapidly via one of the enhanced mechanisms discussed in § 5 would lead to a good agreement with the observed data.

9 Cooling Neutron Stars in Soft X-Ray Transients

Neutron stars undergoing accretion from a companion in a close binary system can also give us information about the state of matter at supranuclear densities. In case of continuous accretion, the bulk of the observable X-ray emission is dominated by the release of gravitational energy when matter hits the neutron star surface and by frictional heating in the inner part of the accretion disc, in case where such a disc exists. Nuclear energy is released during X-ray bursts, and superbursts, which may teach us about the thermal response of the stellar core [118].

A very interesting class of accreting neutron stars consists of the ones in the

so-called Soft X-Ray Transients ("SXRTs") which undergo recurrent surges of activity separated by long phases of relative "quiescence" during which accretion very likely does not occur. The substantial X-ray brightening observed in outburst ($L_{\rm o} \sim 10^{37-38}$ erg s^{-1}) together with type I bursts unambiguously indicate that episodes of intense accretion occur onto a stellar surface, i.e., a neutron star, and not into a black hole. In quiescence, the faint X-ray emission has a luminosity in the order of $L_{\rm q} \sim 10^{31-33}$ erg s^{-1}, i.e., comparable to a standard isolated cooling neutron star. Typically, the duration of an outburst, $t_{\rm o}$, is considerably shorter than the recurrence time between two outbursts, $t_{\rm r}$. In principle, the effects of accretion are the same as in case it is continuous but during the quiescence phase we are most likely detecting thermal emission from the cooling of the neutron star heated up by the accretion. Given the high internal temperature of the star, the heat released in the upper layers from the accretion and the bursts flows back to the surface and is radiated away because of the large temperature gradient in the envelope. Nevertheless, the star stays hot due to energy release from non-equilibrium process in the interior: this heat can be stored in the stellar interior and slowly released when accretion stops.

Non equilibrium processes certainly occur in the crust of an accreting neutron star: thermonuclear processes at the surface will produce iron-peak nuclei which are then pushed to higher densities. In their way, these nuclei will undergo electron capture, neutron emission and absorption and eventually pycnonuclear fusions [119]. Overall, about 1.5 MeV is released as heat for each accreted baryon. This energy is enough to explain the observed quiescent (thermal) luminosities $L_{\rm q}$ in most cases [120]:

$$L_{\rm q} \simeq f \times Q_{\rm nuc} \frac{<\dot{M}>}{m_{\rm u}} \simeq f \times 6 \times 10^{32} \frac{Q_{\rm nuc}}{1.5{\rm MeV}} \, \frac{<\dot{M}>}{10^{-11} M_\odot \ {\rm yr}^{-1}} \ {\rm erg\,s^{-1}}, \quad (23)$$

where $<\dot{M}>$ is the time average of the accretion rate, $Q_{\rm nuc}$ the energy released deep in the crust per accreted baryon, and f the fraction of $Q_{\rm nuc}$ which is stored in the stellar interior, i.e., not lost by neutrino emission. The luminosity $L_{\rm o}$ during an accretion outburst can be estimated as $L_{\rm o} \simeq (\Delta M/t_{\rm o})(GM/R)$ where ΔM is the mass accreted during the outburst. Writing $<\dot{M}> \simeq \Delta M/t_{\rm r}$ one then obtains, following [120],

$$\frac{L_{\rm o} t_{\rm o}}{L_{\rm q} t_{\rm r}} \simeq \frac{GM}{R} \frac{m_{\rm u}}{f Q_{\rm nuc}} \simeq \frac{200}{f} \, . \quad (24)$$

Notice that $L_{\rm o}/L_{\rm q}$ is independent of the source's distance, which is often poorly constrained, while $t_{\rm o}$ and $t_{\rm r}$ can in principle be directly obtained by monitoring the source for a long enough time.

Detailed numerical calculations [121,122] confirmed this simple and elegant picture and are compared with data in Figure 18 (see also [123,124]). Results in this figure are based on a dense matter model in which the direct Urca process is allowed at high densities and controlled by neutron pairing. The

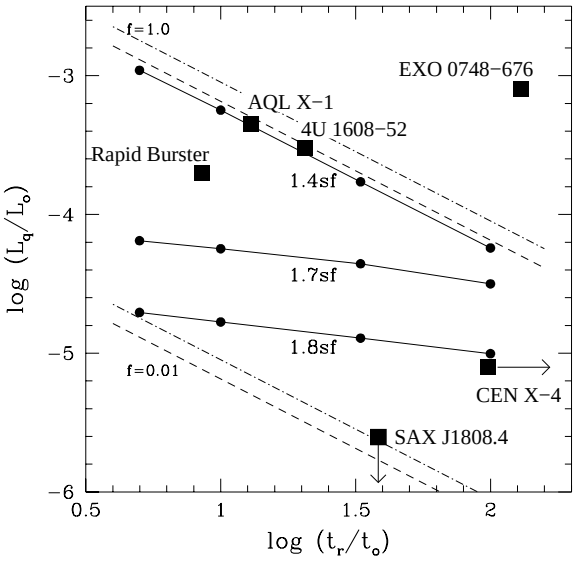

Fig. 18. Quiescent to outburst luminosity ratio plotted versus the recurrence time over the outburst time. The filled squares represent observed values. Estimates for the efficiency of heat storage $f = 1$ and 0.01, Eq. (23) (but with minor GR corrections), are shown for a 1.4 $M_\odot$ star (dashed-dot) and 1.8 $M_\odot$ star (dashed). Dots connected by lines show numerical results (see text) for different neutron star masses as labeled: the 1.4 $M_\odot$ case has no enhanced neutrino emission, i.e., $f \simeq 1$, while the other two cases at 1.7 and 1.8 $M_\odot$ have increasingly more efficient neutrino emission, i.e., $f \ll 1$ (the precise value of the neutron star masses are, however, very model dependent). Adapted from [121], with new data for SAX J1808.4-3658 from [125].

two stars Aql X-1 and 4U 1608–52 show very good agreement with the simple model and the numerical results with $f \simeq 1$, i.e., with negligible neutrino losses and thus very probably are low mass neutron stars. The star in Cen X-4 is noticeably off and seems to require very strong neutrino losses. However, it must be emphasized that in 35 years since its discovery it has undergone only two bursts (in 1969 and 1979) and hence its recurrence time $t_{\rm r}$ is highly uncertain: it is not impossible that this point should be plotted much further to the right, as indicated by the arrow in the figure. The most interesting and intriguing object is certainly SAX J1808.4-3658, dubbed as "The accreting pulsar", which provided the first strong observational evidence for the evolutionary scenario that millisecond pulsars owe their short rotational period to a long phase of accretion in a low mass X-ray binary system. The very low upper limit on its thermal quiescent luminosity $L_{\rm q}$ [125] requires, within the present scenario, very strong neutrino emission (even beyond what has been considered in [121] and shown in Figure 18, i.e., an inner core where enhanced

neutrino emission is not suppressed at all by neutron pairing) and hence a large mass which is in perfect agreement with the idea that recycling of a neutron star to a millisecond rotation period by accretion requires a mass transfer of about 0.2 to 0.5 $M_\odot$ [126]. Notice that the first precise measurement of the mass of a millisecond pulsar, PSR J1909-3744, was recently announced, giving a value of 1.438 ± 0.024 $M_\odot$ [127], at the upper edge of the mass range of binary pulsars [128]. (The latter, which are *not* millisecond pulsars, come from short-lived double massive star systems and did not have time to accreted a significant amount of mass.) The measured mass of PSR J1909-3744 demonstrates that spinning-up of a neutron star to millisecond period does not requires accretion of much more that 0.2 $M_\odot$. Other mass estimates of binary millisecond pulsars [129], though not as accurate, do indicate that much larger masses are reachable, e.g., PSR J0751+1807, which has a mass measurement of $2.1^{+0.4}_{-0.5}$ $M_\odot$ at 95% confidence [130].

Another, and still poorly explored, aspect of these objects is their short timescale thermal response to the accretion phases. This is an aspect of the problem from which extremely important information about both the structure of the neutron star crust and the thermal state of their core can be obtained [122,131], and about which intriguing observational results are being found (see, e.g., [132]).

10 Epilogue and conclusions

Confrontation of the predictions of the Minimal Model with data in § 4 showed a reasonably good agreement with presently available data on isolated cooling neutron star, i.e., no compelling evidence for the occurrence of enhanced neutrino emission is found. Nevertheless, most models of dense matter predict the presence of some form of exotic matter at high enough density, or at least a high proton fraction, which allow enhanced neutrino emission. Are these "non-minimal" scenarios wrong or are we missing cooling neutron stars ?

Before hasting into conclusions, one must first emphasize that the fact the results of the Minimal Cooling scenario are compatible with the data does not mean that the other scenarios are ruled out (unless one is a fervent adept of the "Occam's Razor Principle"). A scientific paradigm is refuted when it is incompatible with experimental facts, not because its competitors are compatible. Alternative scenarios, "exotic" ones or simply with a high proton fraction, whose chemical composition allows enhanced neutrino emission do not necessarily imply fast cooling since the neutrino emission can be suppressed by pairing as we showed in § 5. With large enough gaps these scenarios can be compatible with the data as illustrated in Figure 12. Moreover, enhanced neutrino emission is expected to be allowed, if at all, only at high enough densities,

and hence for sufficiently massive neutron stars, the critical neutron star mass depending on the particular model.

We have no direct information at all about the masses of the observed nearby cooling neutron stars. Many measured masses of radio pulsars in binary systems are between 1.25 to 1.44 $M_\odot$ [128,133]. Exceptions to this are the mass of the binary neutron star J0751+1807 which is in the range $2.1^{+0.4}_{-0.5}$ $M_\odot$ [130], and the companion of PSR J1756-2251, with a mass of $1.18^{+0.03}_{-0.02}$ $M_\odot$ [134]. It is not clear if the mass range of 1.25 to 1.44 $M_\odot$ also applies to *isolated* neutron stars. Evolutionary models of massive stars [135] predict a bimodal distribution for the neutron star masses, with the two peaks being between $1.2 - 1.3$ $M_\odot$ for progenitor main sequences masses below 19 $M_\odot$ (which will burn carbon in a convective core) and between $1.7 - 1.8$ $M_\odot$ for progenitor main sequence masses above 19 $M_\odot$ (where carbon burning will occur in a radiative core). The actual value of 19 $M_\odot$ for the main sequence bifurcation mass may not be very accurate, but the double peaked neutron star mass distribution is certainly real. Given the initial mass function for heavy stars, one could thus expect that massive (e.g., > 1.5 $M_\odot$) isolated neutron stars be very rare.

A neutron star whose temperature is in disagreement with the Minimal Cooling predictions must be of course cold, but moreover young and very likely massive, hence probably uncommon. Therefore, such a star can be expected to be found far away from the Sun and its detection will be very difficult since its weak thermal spectrum will be strongly absorbed. Notice that all young ($<$ a few times 10^4 yrs) neutron stars plotted in Figure 10 are at a distance superior to 1 kpc except for the Vela pulsar. In particular, the two most conspicuous young and cold objects, PSR J0205+6449 (in SNR 3C 58) and RX J0007.0+7302 (in SNR CTA 1) are at distances of 2.6 ± 0.3 kpc and 1.4 ± 0.3 kpc, respectively. Moreover, as emphasized recently in [136], about 80% of the nearby young neutron stars come from the Gould Belt: this local structure of young stellar associations forms a ring of about 1 kpc surrounding the Sun and has an estimated age of 30-50 Myrs. If the Gould Belt's progenitors of the nearby young cooling neutron stars were formed when the belt was formed, which is likely for many of them, and core collapsed about one Myrs ago, they were massive stars not much above 10 $M_\odot$ since heavier stars died well before. From the results of [135] one can safely conclude that most nearby young cooling neutrons stars have masses not exceeding 1.4 $M_\odot$: it is not surprising that none of them shows clear evidence of enhanced neutrino cooling.

The smoking guns in favor of enhanced neutrino cooling are certainly, to date, the two isolated pulsars PSR J0205+6449 and RX J0007.0+7302 (see § 4) and the accreting pulsar SAX J1808.4-3658 (see § 9). Since evolutionary scenarios for recycling pulsar to millisecond periods require accretion of about 0.2 to 0.5 $M_\odot$ [126], SAX J1808.4-3658 is a natural candidate for a neutron star

with an inner core beyond minimal. Possibly more such objects will be found in the SNRs studied recently in [137] (whose present luminosity upper limit are marked as "a", "b", "c", and "d" in Figure 10) in case a neutron star is detected and will provide us with definite evidence for the occurrence of enhanced neutrino emission. Finally, one must entertain the idea that core collapse supernovae fail to produce heavy neutron stars, sending them into a black hole despite their masses are lower than the maximum allowed mass of neutron stars, and that heavy neutron stars can only be found in binary systems, such as SAX J1808.4-3658, after substantial mass accretion occurred.

References

[1] D. G. Yakovlev, C. J. Pethick, Ann. Rev. Astron. Astrophys. 42 (2004) 169.

[2] D. Page, J. M. Lattimer, M. Prakash, A. W. Steiner, Astrophys. J. Suppl. 155 (2004) 623.

[3] G. G. Pavlov, V. E. Zavlin, in: R. Bandiera, R. Maiolino, F Mannucci (Eds.), *Proceedings of the XXI Texas Symposium on Relativistic Astrophysics* (World Sci. Publ. Co. Pte. Ltd, Singapore, 2003), p. 319 [astro-ph/0305435].

[4] F. Haberl, Mem. Soc. Astro. It. 75 (2004) 454 [astro-ph/0401075].

[5] C. Schaab, F. Weber, M. K. Weigel, N. K. Glendenning, Nucl. Phys. A605 (1996) 531.

[6] N. K. Glendenning, *Compact Stars, Nuclear Physics, Particle Physics, and General Relativity*, 2nd ed. (Springer-Verlag, New York, 2000).

[7] F. Weber, *Pulsars as Astrophysical Laboratories for Nuclear and Particle Physics*, High Energy Physics, Cosmology and Gravitation Series (IOP Publishing, Bristol, Great Britain, 1999).

[8] H. Heiselberg, V. Pandharipande, Ann. Rev. Nucl. Part. Sci. 50 (2000) 481.

[9] H. Müther, A. Polls, Prog. Part. Nucl. Phys. 45 (2000) 243.

[10] K. Strobel, F. Weber, M. K. Weigel, Ch. Schaab, Int. J. Mod. Phys. E 6, No. 4 (1997) 669.

[11] R. B. Wiringa, V. Fiks, A. Fabrocini, Phys. Rev. C 38 (1988) 1010.

[12] H. Lenske, C. Fuchs, Phys. Lett. 345B (1995) 355.

[13] C. Fuchs, H. Lenske, H. H. Wolter, Phys. Rev. C 52 (1995) 3043.

[14] S. F. Ban, J. Li, S. Q. Zhang, H. Y. Jia, J. P. Sang, J. Meng, Phys. Rev. C 69 (2004) 045805.

[15] H. Quaintrell *et al.*, Astron. Astrophys. 401 (2003) 313.

[16] J. A. Orosz, E. Kuulkers, Mon. Not. R. Astron. Soc. 305 (1999) 132.

[17] L. Titarchuck and N. Shaposhnikov, Astrophys. J. 570 (2002) L25.

[18] J. M. Weisberg, J. H. Taylor, in: M. Bailes, D. J. Nice, S. E. Thorsett (Eds.), *Radio Pulsars*, ASP Conference Series 302, 2003, p. 93.

[19] C. Alcock, E. Farhi, A. V. Olinto, Astrophys. J. 310 (1986) 261.

[20] N. K. Glendenning, F. Weber, Astrophys. J. 400 (1992) 647.

[21] C. J. Pethick, Rev. Mod. Phys. 64 (1992) 1133.

[22] D. G. Yakovlev, A. D. Kaminker, O. Y. Gnedin, P. Haensel, Phys. Rep. 351 (2001) 1.

[23] D. N. Voskresensky, in: D. Blaschke, N. K. Glendenning, A. Sedrakian (Eds.), *Physics of Neutron Star Interior*, Lect. Notes Phys. 578 (2001), p. 467 [astro-ph/0101514].

[24] J. M. Lattimer, C. J. Pethick, M. Prakash, P. Haensel, Phys. Rev. Lett. 66 (1991) 2701.

[25] M. Prakash, M. Prakash, J. M. Lattimer, C. J. Pethick, Astrophys. J. 390 (1992) L77.

[26] P. Haensel, O. Yu. Gnedin, Astron. Astrophys. 290 (1994) 458.

[27] Ch. Schaab, Master thesis, University of Munich, 1995 (unpublished).

[28] O. Maxwell, G. E. Brown, U. K. Campbell, R. F. Dashen, J. T. Manassah, Astrophys. J. 216 (1977) 77.

[29] G. E. Brown, K. Kubodera, D. Page, P. Pizzochero, Phys. Rev. D 37 (1988) 2042

[30] T. Tatsumi, Prog. Theor. Phys. 80 (1988) 22.

[31] D. Page, E. Baron, Astrophys. J. 354 (1990) L17.

[32] H. Umeda, K. Nomoto, S. Tsuruta, T. Muto, T. Tatsumi, Astrophys. J. 431 (1994) 309.

[33] Ch. Schaab, F. Weber, M. K. Weigel, N. K. Glendenning, Nucl. Phys. A605 (1996) 531.

[34] T. Tatsumi, Prog. Theor. Phys. 69 (1983) 1137.

[35] T. Waas, M. Rho, W. Weise, Nucl. Phys. A617 (1997) 449.

[36] H.-Y. Chiu, E. E. Salpeter, Phys. Rev. Lett. 12 (1964) 413.

[37] B. L. Friman, O. V. Maxwell, Astrophys. J. 232 (1979) 541.

[38] E. N. E. Van Dalen, A. E. L. Dieperink, J. A. Tjon, Phys. Rev. C 67 (2003) 065807.

[39] G. W. Carter, M. Prakash, Phys. Lett. 525 (2002) 249.

[40] D. N. Voskresensky, A. V. Senatorov, Sov. Phys. JETP 63 (1986) 885.

[41] N. Iwamoto, Ann. Phys. 141 (1982) 1.

[42] P. Jaikumar, M. Prakash, Phys. Lett. B516 (2001) 345.

[43] T. Schäfer, K. Schwenzer, Phys. Rev. D 70 (2005) 114037.

[44] U. Lumbardo, H.-J. Schulze, in: D. Blaschke, N. K. Glendenning, A. Sedrakian (Eds.), *Physics of Neutron Star Interior*, Lect. Notes Phys. 578 (2001), p. 30 [astro-ph/0012209].

[45] D. J. Dean, M. Hjorth-Jensen, Rev. Mod. Phys. 75 (2003) 607.

[46] M. Baldo, Ø. Elgarøy, L. Engvik, M. Hjorth-Jensen, H.-J. Schulze, Phys. Rev. C 58 (1998) 1921.

[47] A. Schwenk, B. Friman, Phys. Rev. Lett. 92 (2004) 082501.

[48] K.P. Levenfish, D.G. Yakovlev, Astron. Rep. 38 (1994) 247.

[49] D. G. Yakovlev, A. D. Kaminker, O. Y. Gnedin, P. Haensel, Phys. Rep. 354 (2001) 1.

[50] T. L. Ainsworth, J. Wambach, D. Pines, in: J. Ventura, D. Pines (Eds.), *Neutron Stars: Theory and Observation*, (Kluwer, Dordrecht, 1991) p. 37.

[51] M. V. Zverev, J. W. Clark, V. A. Khodel, Nucl. Phys. A720 (2003) 20.

[52] E. Flowers, M. Ruderman, P. Sutherland, 1976, Astrophys. J. 205 (1976) 541.

[53] D. N. Voskresensky, A. V. Senatorov, Sov. J. Nucl. Phys. 45 (1987) 411.

[54] D. Bailin, A. Love, Phys. Rep. 107 (1984) 325.

[55] D. Bailin, A. Love, J. Phys. A12 (1979) L283.

[56] K. Rajagopal, F. Wilczek, The Condensed Matter Physics of QCD, in: M. Shifman (Ed.), *At the Frontier of Particle Physics / Handbook of QCD* (World Scientific, Singapore, 2001) [hep-ph/0011333].

[57] M. Alford, Ann. Rev. Nucl. Part. Sci. 51 (2001) 131.

[58] K. Rajagopal, F. Wilczek, Phys. Rev. Lett. 86 (2001) 3492.

[59] K. Nomoto, S. Tsuruta, Astrophys. J. 312 (1987) 711.

[60] J. M. Lattimer, K. A. van Riper, M. Prakash, M. Prakash, Astrophys. J. 425 (1994) 802.

[61] O. Y. Gnedin, D. G. Yakovlev, A. Y. Potekhin, Mon. Not. R. Astron. Soc. 324 (2001) 725.

[62] P. Jaikumar, C. Gales, D. Page, submitted to Phys. Rev. D. [hep-ph/0508245].

[63] E. H. Gudmundsson, C. J. Pethick, R. I. Epstein, Astrophys. J. 259 (1982) L19.

[64] E. H. Gudmundsson, C. J. Pethick, R. I. Epstein, Astrophys. J. 272 (1983) 286.

[65] G. Greenstein, G. J. Hartke, Astrophys. J. 271 (1983) 283.

[66] D. Page, Astrophys. J. 442 (1995) 273.

[67] D. Page, A. Sarmiento, Astrophys. J. 473 (1996) 1067.

[68] G. Chabrier, A.Y. Potekhin, D.G. Yakovlev, Astrophys. J. 477 (1997) L99.

[69] D. G. Yakovlev, V.A. Urpin, Sov. Astron. 24 (1980) 303.

[70] A. Y. Potekhin, G. Chabrier, D. G.Yakovlev, Astron. Astrophys. 323 (1997) 415.

[71] A.Y. Potekhin, D.G. Yakovlev, Astron. Astrophys. 374 (2001) 213.

[72] T. Takatsuka, Prog. Theor. Phys. 48 (1972) 1517.

[73] L. Amundsen, E. Østgaard, Nucl. Phys. A437 (1985) 487.

[74] M. E. Gusakov, A. D. Kaminker, D. G. Yakovlev, D. Y. Gnedin, Astron. Astrophys. 423 (2004) 1063.

[75] D. Page, Ph.D. dissertation, SUNY at Stony Brook, 1989 (unpublished).

[76] D. Page, J. H. Applgate, Astrophys. J. 394 (1992) L17.

[77] H. Umeda, K. Nomoto, S. Tsuruta, T. Muto, T. Tatsumi, Astrophys. J. 431 (1994) 309.

[78] S. Tsuruta, M. A. Teter, T. Takatsuka, T. Tatsumi, R. Tamagaki, Astrophys. J. 571 (2002) L143.

[79] D. Page, in: N. Shibazaki, N. Kawai, S. Shibata, T. Kifune (Eds.), *Neutron Stars and Pulsars: thirty years after the discovery* (Universal Academy Press, Tokio, 1998), p. 183 [astro-ph/9802171].

[80] C. Schaab, S. Balberg, J. Schaffner-Bielich, Astrophys. J. 504 (1998) L99.

[81] D. Page, M. Prakash, J.M. Lattimer, A.W. Steiner, Phys. Rev. Lett. 85 (2000) 2048.

[82] C. Schaab, D. Voskresensky, A. D. Sedrakian, F. Weber, M. K. Weigel, Astron. Astrophys. 321 (1997) 591.

[83] G. G. Pavlov, G. S. Stringfellow, F. A. Cordova, Astrophys. J. 467 (1996) 370.

[84] N. K. Glendenning, Ch. Kettner, F. Weber, Astrophys. J. 450 (1995) 253.

[85] N. K. Glendenning, Ch. Kettner, F. Weber, Phys. Rev. Lett. 74 (1995) 3519.

[86] F. Weber, Prog. Part. Nucl. Phys. 54 (2005) 193.

[87] D. Page, in: R. Huerta, M. A. Perez (Eds), *High Energy Phenomonology* (World Scientific, Singapore, 1992), p. 347 [astro-ph/9602043].

[88] K. Rajagopal, F. Wilczek, Phys. Rev. Lett. 86 (2001) 3492.

[89] V. V. Usov, Phys. Rev. D 70 (2004) 067301.

[90] P. Jaikumar, M. Prakash, T. Schäfer, Phys. Rev. D 66 (2002) 063003.

[91] I. A. Shovkovy, P. J. Ellis, Phys. Rev. C 66 (2002) 015802.

[92] H. Grigorian, D. Blaschke, D. Voskresensky, Phys. Rev. C 71 (2005) 045801.

[93] S. E. Woosley, E. Baron, Astrophys. J. 391 (1992) 228; S. E. Woosley, Astron. Astrophys. 97 (1993) 205.

[94] V. V. Usov, Astrophys. J. 481 (1997) L107.

[95] C. Kettner, F. Weber, M. K. Weigel, N. K. Glendenning, Phys. Rev. D 51 (1995) 1440.

[96] V. V. Usov, Phys. Rev. Lett. 80 (1998) 230.

[97] V. V. Usov, Astrophys. J. 550 (2001) L179.

[98] A. Aksenov, M. Milgrom, V. V. Usov, Mon. Not. R. Astron. Soc. 343 (2003) L69; Astrophys. J. 609 (2004) 363.

[99] P. Jaikumar, C. Gale, D. Page, M. Prakash, Phys. Rev. D 70 (2004) 023004.

[100] D. Page, V. V. Usov, Phys. Rev. Lett. 98 (2002) 131101; see also `http://focus.aps.org/story/v10/st13`.

[101] U. Geppert, M. Kueker, D. Page, Astron. Astrophys. 416 (2004) 257.

[102] D. Page, M. Kueker, U. Geppert, in preparation.

[103] C. Thompson, R. C. Duncan, Astrophys. J. 473 (1996) 322.

[104] M. Colpi, U. Geppert, D. Page, Astrophys. J. 529 (2000) L29.

[105] P. Arras, A. Cumming, C. Thompson, Astrophys. J. 608 (2004) L49.

[106] D. Page, U. Geppert, T. Zannias, Astron. Astrophys. 360 (2000) 1052.

[107] V. Urpin, D. Konenkov, Mon. Not. R. Astron. Soc. 292 (1997) 167.

[108] P. Goldreich, A. Reisenegger, Astrophys. J. 395 (1992) 250.

[109] M. Rheinhardt, U. Geppert, Phys. Rev. Lett. 88 (2002) 101103.

[110] U. Geppert, M. Rheinhardt, J. Gil, Astron. Astrophys. 412 (2003) L33.

[111] Ch. Schaab, A. Sedrakian, F. Weber, M. K. Weigel, Astron. & Astrophys. 346 (1999) 465.

[112] P. Haensel, Astron. Astrophys. 262 (1992) 131.

[113] A. Reisenegger, P. Goldreich, Astrophys. J. 395 (1992) 240.

[114] K. Iida, K. Sato, Astrophys. J. 477 (1997) 294.

[115] A. Reisenegger, Astrophys. J. 485 (1997) 313.

[116] D. Page, Astrophys. J. 479 (1997) L43

[117] H. Umeda, N. Shibazaki, K. Nomoto, S. Tsuruta, Astrophys. J. 408 (1993) 186.

[118] E. Rehm, H. Schatz, this volume (2004).

[119] P. Haensel, J. L. Zdunik, Astron. Astrophys. 227 (1990) 431; Astron. Astrophys. 404 (2003) L33.

[120] E. F. Brown, L. Bildsten, R. E. Rutledge, Astrophys. J. 504 (1998) L95.

[121] M. Colpi, U. Geppert, D. Page, A. Possenti, Astrophys. J. 548 (2001) L175.

[122] G. Ushormirsky, R. E. Rutledge, Mon. Not. R. Astron. Soc. 325 (2001) 1157.

[123] D. G. Yakovlev, K. P. Levenfish, P. Haensel, Astron. Astrophys. 407 (2003) 265.

[124] D. G. Yakovlev, K. P. Levenfish, A. Y. Potekhin, O. Y. Gnedin, G. Chabrier, Astron. Astrophys. 417 (2004) 169.

[125] S. Campana *et al.*, Astrophys. J. 575 (2002) L15.

[126] G. B. Cook, S. L. Shapiro, S. A Teukolsky, Astrophys. J. 423 (1994) L117.

[127] B. A. Jacoby, A. Hotan, M. Bailes, S. Ord, S. R. Kulkarni, Astrophys. J., in press (2005) [astro-ph/0507420].

[128] S. E. Thorsett, D. Chakrabarty, Astrophys. J. 512 (1999) 288.

[129] D. J. Nice, E. M. Splaver, I. H. Stairs, in: F. A. Rasio, I. H. Stairs (Eds.), *Binary Radio Pulsars*, ASP Conference Series, 302 (2003), p. 75 [astro-ph/00411207].

[130] D. J. Nice, E. M. Splaver, I. H. stairs, O. Lömer, A. Jessner, M. Kramer, J. M. Cordes, Astrophys. J., submitted [astro-ph/0508050]

[131] E. F. Brown, L. Bildsten, P. Chang, Astrophys. J. 574 (2002) 920.

[132] R. Wijnand, J. Homan, J. M. Miller, W. H. G. Lewin, Astrophys. J. 606 (2004) L62.

[133] A. G. Lyne *et al.*, Science 303 (2004) 1153.

[134] A. J. Faulkner *et al.*, Astrophys. J. 618 (2005) L119.

[135] F. X. Timmes, S. E. Woosley, T. Weaver, Astrophys. J. 457 (1996) 834.

[136] S. B. Popov, M. Colpi, M. E. Prokhorov, A. Treves, R. Turolla, Astron. Astrophys. 406 (2003) 111.

[137] D. L. Kaplan, D. A. Frail, B. M. Gaensler, E. V. Gotthelf, S. R. Kulkarni, P. O. Slane, A. Nechita, Astrophys. J. Suppl. 153 (2004) 269.